The FEBS Journal

FEBS PRESS science publishing by scientists

TRIM32 controls timely cell cycle exit in muscular differentiation through downregulation of c-Myc mRNA

Lu Xiong[1], Elisa Lazzari[1], Sabrina Pacor[1], Simeone Dal Monego[2], Erica Piovesan[1], Danilo Licastro[2] and Germana Meroni[1]

1 Department of Life Sciences, University of Trieste, Italy
2 AREA Science Park, Trieste, Italy

Keywords
c-Myc; LGMDR8; muscular dystrophy; myogenesis; TRIM32

Correspondence
G. Meroni, Department of Life Sciences, University of Trieste, Via L. Giorgieri 5, 34127 Trieste, Italy
Tel: +390405588679
E-mail: gmeroni@units.it

(Received 12 December 2025, revised 2 April 2026, accepted 4 June 2026)

doi:10.1111/febs.70619

Mutations in *TRIM32* cause limb-girdle muscular dystrophy recessive 8 (LGMDR8), a neuromuscular disorder primarily affecting the proximal muscles of hips and shoulders. However, the precise pathogenic mechanism remains unclear. In this study, we used *Trim32* knock-out C2C12 murine myoblasts to investigate the impact of full *Trim32* loss along the myogenesis process. We found that *Trim32* deficiency alters global transcriptomics already in the early phases of the differentiation process leading to impaired myogenic signaling, ultimately resulting in delayed and abnormal myotube formation. Following this up, we discovered that lack of Trim32 disrupts the transition from proliferation to differentiation by limiting the necessary downregulation of the proto-oncogene c-Myc, thus delaying and altering the immediate early onset of differentiation. Interestingly, unlike previous reports that emphasized protein-level regulation, our data reveal that, at this precise stage of differentiation, Trim32 regulates the stability of c-Myc at mRNA level. Attenuating c-Myc expression level is able to partially recover the myogenesis defects observed in the absence of Trim32, suggesting that the Trim32–c-Myc axis may represent an essential hub, although likely not the exclusive mechanism, in muscle regeneration within LGMDR8 pathogenesis.

Introduction

Tripartite motif-containing protein 32 (*TRIM32*) was originally identified as a zinc finger protein interacting with the activation domain of lentiviral Tat proteins [1]. Structurally, TRIM32 contains a conserved N-terminal module, the tripartite motif, comprising a RING domain, a single type 2 B-box domain, and a Coiled-Coil region, while its C-terminal portion features a six-bladed β-propeller NHL domain [2]. The RING domain is responsible for the E3 ligase catalytic function [3,4] and indeed TRIM32 is primarily known for its function as an E3 ubiquitin ligase [5]. Within the tripartite motif, the precise role of the B-box domain remains unclear, although some studies suggest that it modulates the rate of ubiquitin chain assembly [6], while the Coiled-Coil domain facilitates, together with the RING domain, TRIM32

Abbreviations
ACTA1, α-actin 1; ACTN2, α-actinin 2; Adm, adrenomedullin; BSA, bovine serum albumin; Ccnb1, cyclin B1; CFSE, carboxyfluorescein diacetate succinimidyl ester; CHX, cycloheximide; DEGs, differentially expressed genes; DES, desmin; DM, differentiation medium; DMSO, dimethyl sulfoxide; DTT, DL-dithiothreitol; EDTA, ethylenediaminetetraacetic acid; EU, 5-ethynyl uridine; FDR, false discovery rate; GM, growth medium; KO, knock-out; LGMDR8, limb-girdle muscular dystrophy recessive 8; MDS, multidimensional scaling; MRFs, myogenic regulatory factors; MuSC, muscular stem cells; MyHC, myosin heavy chain; PAGE, polyacrylamide gels; PBS, phosphate-buffered saline; PFA, paraformaldehyde; pHH3, phospho-histone H3; PI, propidium iodide; PMSF, phenylmethylsulfonyl fluoride; Rcl, RNA terminal phosphate cyclase like 1; SDS, sodium dodecyl sulfate; TBST, tris buffered saline with 0.1% Tween; Tert, telomerase reverse transcriptase; TMOD1, tropomodulin 1; Tnbs1, thrombospondin 1; Trim32, tripartite motif-containing protein 32; TTN, titin; WT, wild-type.

homo-oligomerization that is essential for its activity [7]. The NHL domain plays a crucial role in protein–protein interactions, likely conferring substrate specificity [8]. Additionally, the NHL domain has also been shown to interact with RNA and growing evidence revealed that, in addition to its E3 ligase activity, TRIM32 is implicated in RNA-mediated regulation [9–12].

Mutations in *TRIM32* result in an inherited rare neuromuscular disorder, Limb-Girdle Muscular Dystrophy recessive 8 (LGMDR8) [13–15]. This disease is characterized by the progressive wasting of muscles, mainly manifesting in the proximal muscles of the arms and legs [16]. LGMDR8-associated mutations are distributed across different domains of TRIM32, with the NHL domain being the most commonly affected [17]. Additionally, cases with full deletion of TRIM32 have been reported [18,19]. Patients carrying mutations in the NHL domain exhibit an abnormal low level of TRIM32 in muscle tissue, likely due to decreased TRIM32 protein stability [20,21]. Knock-in mice carrying an LGMDR8 corresponding pathogenic mutation (p.Asp489Asn) also presented reduced levels of mutated Trim32 protein but levels of RNA expression comparable to wild-type (WT) animals, further suggesting that mutations in Trim32 alter its protein stability. Both the knock-in and full *Trim32* knock-out animal models presented a mild myopathy phenotype and both recapitulate the human phenotype [22,23]. This evidence strongly indicates that LGMDR8 is caused by the loss of TRIM32 function.

LGMDR8 pathogenesis is not totally unraveled and reported findings support a role for TRIM32 in both muscle atrophy and regeneration. Early studies primarily focused on the role of TRIM32 in muscle atrophy, identifying several sarcomeric structural proteins, including actin, α-actinin, tropomyosin, desmin, and dysbindin, as potential substrates of TRIM32 E3 ubiquitin ligase activity assessed *in vitro* [24–26]. However, it remains unclear whether TRIM32 plays a fundamental role in promoting atrophy and how this would be relevant for LGMDR8 pathogenesis. On the other hand, increasing evidence from both patient-derived samples and *Trim32*-deficient mouse models suggests that TRIM32 is critically involved in muscle regeneration, indicating that its role in LGMDR8 pathogenesis may extend beyond sarcomeric protein degradation and involve broader regulation of muscle homeostasis, including a role in regulation of the myogenic process [21,23,27,28]. Myogenesis is a highly complex physiological process involving extensive crosstalk between multiple signaling pathways that collectively regulate myoblast proliferation, fusion, and differentiation [29–32]. Notably, TRIM32 is expressed at higher levels in myoblasts than in mature skeletal muscle tissue and its expression is significantly increased during muscle regeneration after injury [22,27,28]. These observations prompted extensive research into the role of TRIM32 in myoblast differentiation; however, although there is no doubt that TRIM32 is necessary for full myogenesis, there are still inconsistencies in the reported data regarding the molecular processes and the stage(s) of TRIM32 requirement within muscular regeneration. As examples, both reduced and increased numbers of satellite cells, the adult muscular stem cells (MuSC), have been reported in *Trim32* knock-out animal models [27,28] and, in myoblast cellular systems, both pro-proliferative as well as antiproliferative effects, including senescence, have been proposed in TRIM32-related models [21,27,28]. In addition, as the analyses have been performed in different experimental settings and with a focus either in myoblast proliferating state or after the induction of differentiation, it is difficult to converge toward a unifying mechanism. Further, we cannot rule out the possibility that TRIM32 might play different roles in diverse stages of myogenesis.

Instead, a role of TRIM32 in negatively regulating stemness and favoring differentiation has been more extensively studied in neuronal cells. In this context, TRIM32-mediated proteasomal degradation of c-Myc has been reported to be implicated [12,33–35]. An analogous role was proposed in the muscular system; however, no solid evidence associates c-Myc accumulation and its TRIM32-mediated ubiquitination with the myogenesis defect [28].

Thus, despite the increasing body of evidence placing TRIM32 as a central regulator of myogenesis, it is still poorly understood how its mutations may affect this process resulting in LGMDR8 [17,36,37]. In this study, we employed a more homogeneous system generating *Trim32* knock-out in the C2C12 myoblast cell line to comprehensively characterize myogenesis upon loss of Trim32 and dissect its role along the process from myoblasts to myotube formation. We confirmed that the absence of Trim32 dramatically impairs C2C12 myogenesis, having a broad impact on the transcriptome of differentiating cells and inhibiting the expression of key myogenic proteins. This impairment originates at the very onset of the differentiation stimulus, at which time *Trim32* knock-out myoblasts are unable to properly exit from the cell cycle, likely due to inefficient downregulation of the messenger RNA of the pro-proliferative c-Myc oncogene.

Results

Absence of Trim32 impairs differentiation of C2C12 cells

To investigate the role of Trim32 in muscular differentiation, the immortalized mouse myoblast cell line C2C12 was selected for its robust myogenic capacity [38,39]. Under high-serum conditions, these myoblasts proliferate effectively, while in low-serum conditions, they start the myogenic process, differentiating and fusing into myotubes [40].

We generated *Trim32* knock-out (*Trim32* KO) C2C12 myoblasts using CRISPR/Cas9-mediated gene editing (Fig. 1A). Three independent single-cell *Trim32* KO clones were selected for subsequent experiments: two homozygous (c.49delG; p.E17Kfs*1) and one compound heterozygous (c.22_61del and c.49_50insG; p.S8Vfs*52 and p.E17Gfs*12) (Fig. 1B and Table 1). All these mutations result in frameshifts generating premature stop codons and leading to the expression of nonfunctional very short N-terminal truncated Trim32 protein, if any, and the absence of the Trim32 protein in KO clones was confirmed with western blot analysis using two polyclonal antibodies targeting either the N-terminal (Fig. 1C) or the central regions (data not shown) of Trim32. Given that C2C12 cells differentiation potential could be affected by prolonged subculturing during gene editing procedure, we opted to use 3 *Trim32* wild-type (WT) clones, besides the original parental C2C12 cells, as control for all subsequent analyses; these clones underwent the same editing and selection protocol as the *Trim32* KO but resulted wild-type for *Trim32* (WT) (Table 1).

Having generated *Trim32* KO C2C12 clones, we started assessing the differentiation of these cells in culture. Myogenesis is a tightly regulated process that is achieved by timely controlled expression of myogenic regulatory factors (MRFs), which ultimately regulate expression of myosin heavy chain (MyHC), a structural protein of the sarcomere exclusively expressed in differentiating myocytes and myotubes [41,42]. In the classic differentiation protocol, C2C12 cells are grown in proliferating medium (growth medium, GM) and then triggered to differentiate upon serum reduction (differentiation medium, DM) (see Methods and upper scheme of Fig. 1D). Using Myosin Heavy Chain 3 (MyHC) as a marker to monitor C2C12 differentiation, we could observe that by day 8 (D8) WT clones showed formation of myotubes to a similar extent as parental C2C12, while *Trim32* KO clones appeared severely impaired in their ability to generate myotubes. Additionally, the myotubes formed by *Trim32* KO clones were significantly smaller, exhibited clustered nuclei, and lacked the proper elongated, stretched morphology observed in WT myotubes (Fig. 1D). Interestingly, impairment of the differentiation program in *Trim32* KO clones is apparent already at early stages: at day 3 (D3) of differentiation in fact we observed a complete absence of MyHC-expressing cells in the *Trim32* KO clones, while WT and parental cells already display formation of myotube precursors at this differentiation stage (Fig. 1D).

Analysis of one of the upstream regulators of MyHC expression, myogenin, further confirmed aberrant differentiation in the absence of Trim32. Elevated myogenin levels are observed in myoblasts that exit the cell cycle and differentiate into myotubes [43]. Indeed, *Trim32* KO clones showed markedly reduced Myogenin-positive cells after 8 days of differentiation, consistent with reduced differentiation potential into myotubes. Interestingly, the residual myogenin-positive cells did not correspond to the few and abnormal myotubes formed by *Trim32* KO clones, whereas myogenin was abundantly detected in the nuclei of WT and parental C2C12 myotubes (Fig. 1D). The aberrant differentiation of *Trim32* KO clones was confirmed by determining the differentiation index: compared to an average of 13.99% of nuclei within MyHC-positive myotubes in WT clones, the percentage was only 3.68% in *Trim32* KO cells after full-term differentiation (D8) (Fig. 1E). Overall impaired upregulation of differentiation markers was also assessed by western blot analysis showing reduced expression of both MyHC and Myogenin (Fig. 1F) in *Trim32* KO clones after 8 days of differentiation (D8), consistent with the observed defect in myotube formation in *Trim32* KO cells.

These results indicate the critical requirement of Trim32 for C2C12 myoblast myogenesis and confirm, as reported previously, that deletion of *Trim32* causes myogenic defects without completely eliminating myotube formation in C2C12 cells.

Transcriptomic analysis of Trim32 WT and Trim32 KO clones along early differentiation

Based on our initial observations, the absence of Trim32 already exerts a significant impact by day 3 (D3) of C2C12 myogenic differentiation. To investigate how Trim32 influences early global transcriptional changes during the proliferative phase (D0) and early differentiation (D3), we performed an unbiased transcriptomic profiling of WT and *Trim32* KO clones (Fig. 2A). Multidimensional Scaling (MDS) analysis revealed clear segregation of gene expression profiles

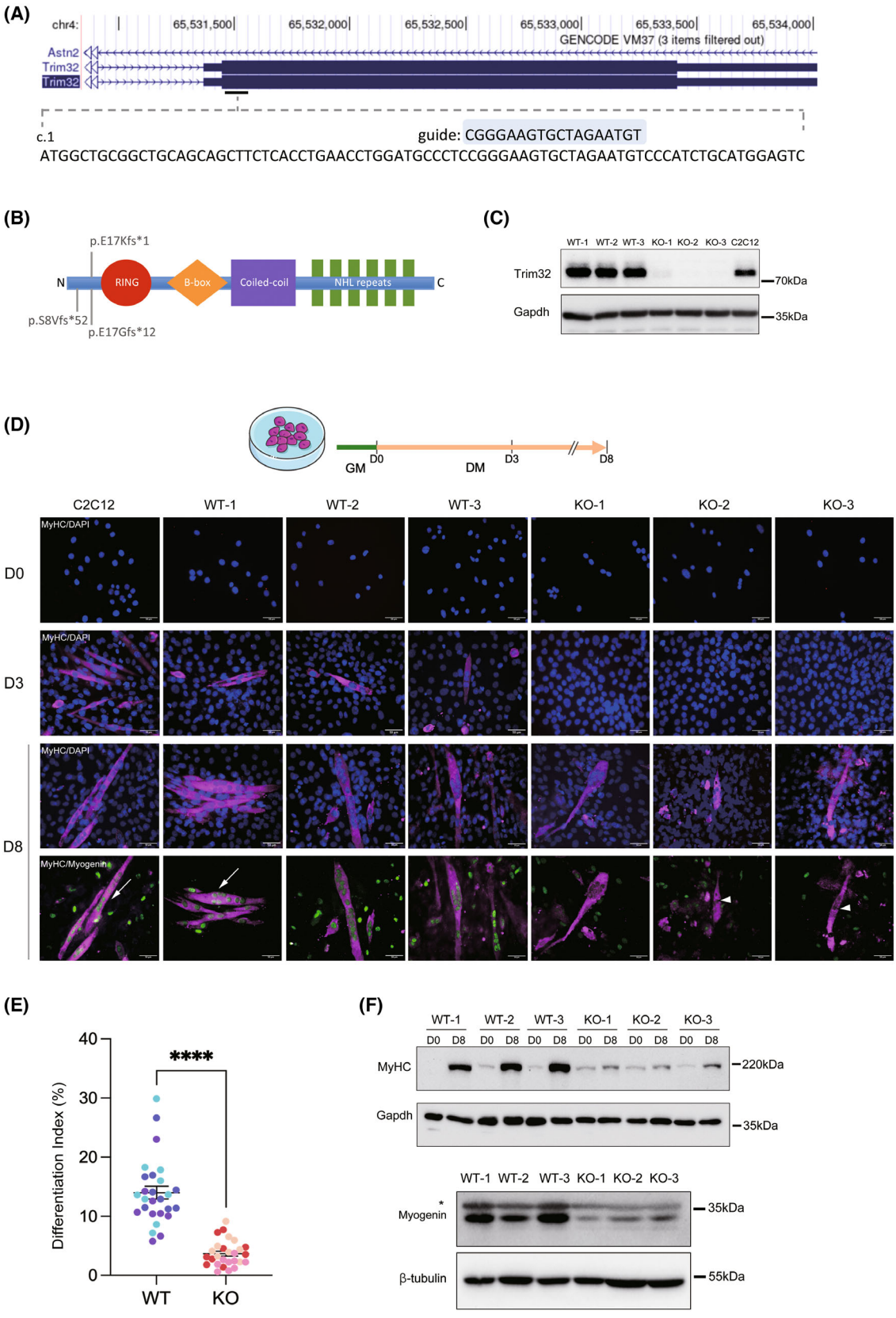

Fig. 1. Myogenesis is impaired in *Trim32* knock-out (KO) cells. (A) Diagram illustrating the structure of the mouse *Trim32* gene and the positions of the designed gRNA on the 5′ *Trim32* coding sequence. (B) Scheme of the *Trim32* mutations generated in C2C12 and resulting in premature stop codons and leading to nonfunctional fragments: p.E17Kfs*1, p.S8Vfs*52 and p.E17Gfs*12. (C) Representative western blot of Trim32 in parental C2C12 cells, three *Trim32* KO clones, and three wild-type (WT) clones ($n = 3$). Trim32 protein was detected using an antibody against its N terminus. (D) Top, scheme of the differentiation timeline adopted. Bottom, immunostaining for myosin heavy chain 3 (MyHC) (magenta) at day 0 (D0), and at 3 (D3) and 8 days (D8) of differentiation, in parental C2C12 cells, 3 WT clones and 3 *Trim32* KO clones. At D8 double staining for Myogenin (green) is shown. Arrows indicate Myogenin-positive nuclei in myotubes of WT and parental C2C12; arrowheads indicate nuclei lacking Myogenin expression in *Trim32* KO myotubes. Nuclei were counterstained with DAPI (blue) (Scale bar = 50 μm; magnification 40×; $n = 3$). (E) Differentiation index of *Trim32* KO and WT clones at D8. The differentiation index is calculated as the ratio of nuclei within MyHC-positive myotubes to the total number of nuclei (mean ± SD; unpaired *t*-test, ****$P < 0.0001$; $n = 3$). Each dot represents a 20× microscope field (3 fields × 3 coverslips were analyzed for each clone); shades of blue and red represent the different clones (F) Top, representative western blot of MyHC protein levels in *Trim32* WT and KO clones at D0 and D8 of differentiation as indicated ($n = 3$). Gapdh was used as loading control. Bottom, representative western blot of Myogenin protein levels in *Trim32* KO and WT clones at D8 of differentiation ($n = 3$). Asterisk indicates a nonspecific band. β-tubulin was used as loading control. Experiments were repeated three times.

Table 1. Genotypes of the generated C2C12 clones.

	Clones	*Trim32* genotype	*Trim32* mutations
Trim32 KO	KO-1	c.49delG/c.49delG	p.E17Kfs*1
	KO-2	c.49delG/c.49delG	p.E17Kfs*1
	KO-3	c.22_61del/ c.49_50insG	p.S8Vfs*52/ p.E17Gfs*12
WT	WT-1	WT	None
	WT-2	WT	None
	WT-3	WT	None

based on both time of differentiation (Dim1, 44% variance) and *Trim32* genotype (Dim2, 16% variance) (Fig. 2A). Likewise, hierarchical clustering grouped WT and *Trim32* KO clones into distinct clusters at both timepoints, indicating consistent genotype-specific transcriptional differences (data not shown). Differentially Expressed Genes (DEGs) were detected in the *Trim32* KO transcriptome relative to WT, at both D0 and D3. In proliferating conditions, 72 genes were upregulated and 189 were downregulated whereas at D3 of differentiation, 72 genes were upregulated and 212 were downregulated. Ingenuity pathway analysis of the DEGs revealed the top 10 canonical pathways as enriched at either D0 or D3 (Fig. 2B). Several of these pathways can underscore relevant Trim32-mediated functions though most of them represent generic functions not immediately attributable to the observed myogenesis defects.

Notably, the transcriptional divergence between WT and *Trim32* KO cells is more pronounced at D3, as evidenced by a greater separation along the MSD Dim2 axis, suggesting that Trim32-dependent transcriptional regulation intensifies during early differentiation (Fig. 2A). Given our interest in the differentiation process, we therefore focused our analyses comparing the changes occurring from D0 to D3 in WT (WT D3 vs. D0) and in *Trim32* KO (KO D3 vs. D0) RNAseq data.

Pathway enrichment analysis of D3 vs. D0 DEGs allowed the selection of the top-scored pathways for both WT and *Trim32* KO data. We obtained 18 top-scored pathways enriched in each genotype ($-\log(P\text{-value}) \geq 9$ cut-off): 14 are shared while 4 are top-ranked only in WT and 4 only in *Trim32* KO (Fig. 2C). For the following analyses, we employed thus a total of 22 distinct pathways and to better mine those relevant in the passage from the proliferation stage to the early differentiation one and that are affected by the lack of Trim32, we built a bubble plot comparing side-by-side the scores and enrichment of the 22 selected top-scored pathways above in WT and *Trim32* KO (Fig. 2D). A heatmap of DEGs included within these selected pathways confirms the clustering of the samples considering both the genotypes and the timepoints highlighting gene expression differences (Fig. 2E). These pathways are mainly related to muscle development, cell cycle regulation, genome stability maintenance and few other metabolic cascades.

As expected given the results related to Fig. 1, moving from D0 to D3 WT clones showed robust upregulation of key transcripts associated with the Inactive Sarcomere Protein Complex, a category encompassing most genes in the 'Striated Muscle Contraction' pathway, while in *Trim32* KO clones this pathway was not among those enriched in the transition from D0 to D3 (Fig. 2C). Detailed analyses of transcripts enclosed within this pathway revealed that on the transition from proliferation to differentiation, WT clones show upregulation of several Myosin Heavy Chain isoforms (e.g., *MYH3, MYH6, MYH8*), α-Actin 1 (*ACTA1*), α-Actinin 2 (*ACTN2*), Desmin (*DES*), Tropomodulin 1 (*TMOD1*), and Titin (*TTN*), a pattern consistent with previous reports, while these same transcripts were

(A)

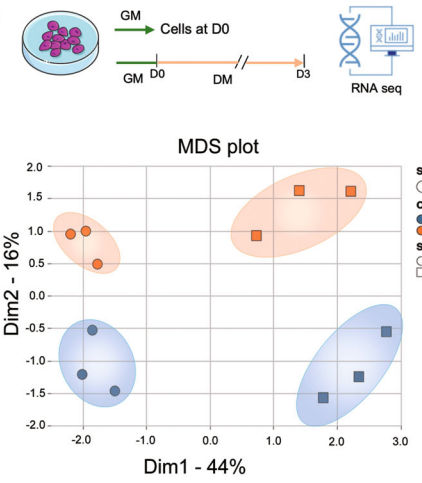

(B)

D0 WT *vs* KO	Ingenuity top Canonical Pathways	-log(p-value)	z-Score	Ratio
	Hepatic Fibrosis / Hepatic Stellate Cell Activation	5.61		0.0567
	CREB Signaling in Neurons	4.72	2.83	0.0297
	Axonal Guidance Signaling	4.55		0.0315
	Breast Cancer Regulation by Stathmin1	4.28	2.18	0.0286
	Hepatic Fibrosis Signaling Pathway	3.72	1.13	0.0309
	Osteoarthritis Pathway	3.38	0	0.0381
	Regulation of the Epithelial-Mesenchymal Transition Pathway	3.27		0.041
	Netrin Signaling	3.23	0.45	0.0694
	Cardiac Hypertrophy Signaling (Enhanced)	3.18	0.63	0.0258
	Amyotrophic Lateral Sclerosis Signaling	3.11		0.0522

D3 WT *vs* KO	Ingenuity top Canonical Pathways	-log(p-value)	z-Score	Ratio
	Calcium Signaling	8.76	1.89	0,0734
	Actin Cytoskeleton Signaling	8.03	2.71	0,0653
	Oxytocin Signaling Pathway	8.00	2.67	0,0605
	Cellular Effects of Sildenafil (Viagra)	7.15		0,0805
	ILK Signaling	6.61	2.50	0,065
	Phagosome Formation	6.38	2.86	0,0347
	PAK Signaling	6.26	2.12	0,0847
	G-Protein Coupled Receptor Signaling	6.24	2.04	0,0341
	Semaphorin Neuronal Repulsive Signaling Pathway	6.16	1.00	0,0728
	Dilated Cardiomyopathy Signaling Pathway	5.36	-2.33	0,0676

(C)

Ingenuity Canonical Pathways			
WT - D3 *vs* D0	**-log(p-value)**	**KO - D3 *vs* D0**	**-log(p-value)**
Cell Cycle Checkpoints	29.9	Cell Cycle Checkpoints	38.9
Mitotic Prometaphase	19.8	Mitotic Prometaphase	24.0
Mitotic Metaphase and Anaphase	18.7	Activation of the pre-replicative complex	21.5
RHO GTPases Activate Formins	18.0	HDR through Homologous Recombination (HRR) or Single Strand Annealing (SSA)	20.1
Kinetochore Metaphase Signaling Pathway	15.7	Mitotic Metaphase and Anaphase	20.0
Activation of the pre-replicative complex	14.4	RHO GTPases Activate Formins	18.8
Cell Cycle Control of Chromosomal Replication	14.0	Cell Cycle Control of Chromosomal Replication	17.1
HDR through Homologous Recombination (HRR) or Single Strand Annealing (SSA)	13.1	Kinetochore Metaphase Signaling Pathway	16.5
Hereditary Breast Cancer Signaling	12.6	Hereditary Breast Cancer Signaling	16.1
Nuclear Cytoskeleton Signaling Pathway	12.4	Role of BRCA1 in DNA Damage Response	15.3
Role of BRCA1 in DNA Damage Response	12.0	Synthesis of DNA	14.2
Hepatic Fibrosis / Hepatic Stellate Cell Activation	11.9	Telomere Maintenance	11.8
Extracellular matrix organization	11.3	Cholesterol biosynthesis	11.8
Pulmonary Fibrosis Idiopathic Signaling Pathway	11.1	Mismatch Repair in Eukaryotes	11.5
Striated Muscle Contraction	11.0	Nuclear Cytoskeleton Signaling Pathway	11.5
Synthesis of DNA	10.1	Role of CHK Proteins in Cell Cycle Checkpoint Control	10.8
Axonal Guidance Signaling	9.33	Regulation of TP53 Activity through Phosphorylation	10.5
Regulation of TP53 Activity through Phosphorylation	9.17	Hepatic Fibrosis / Hepatic Stellate Cell Activation	10.4

(D)

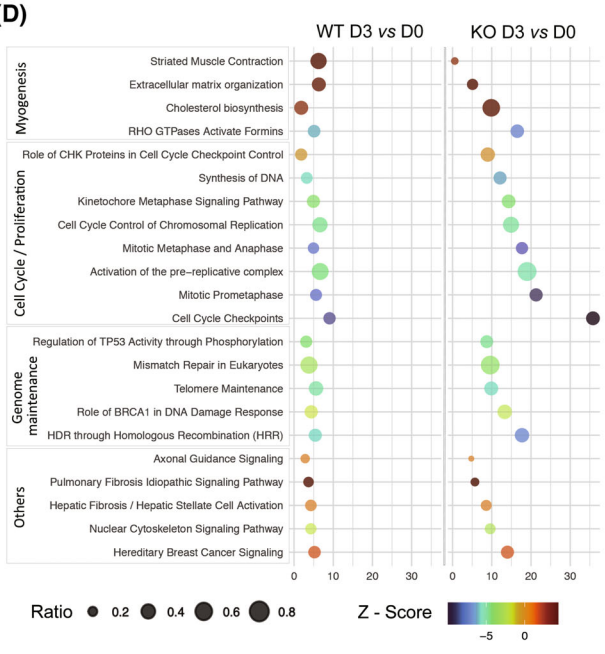

(E)

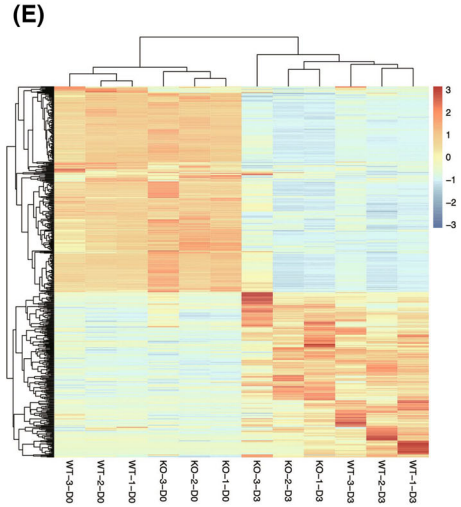

Fig. 2. Transcriptomic analysis reveals defective myogenesis and proliferation programs in *Trim32* knock-out (KO) cells. (A) Scheme of cellular differentiation for the RNAseq experiment and multidimensional scaling (MDS) analysis of RNAseq data from three *Trim32* KO and three wild-type (WT) clones in proliferation (D0) and differentiation (D3) conditions. Dim1: time of differentiation; Dim2: *Trim32* genotype. Genotypes and time points are indicated in the graph with color and shape code, respectively. (B) List of the 10 top-ranked enriched Ingenuity canonical pathways in WT vs *Trim32* KO differentially expressed genes (DEGs) at D0 (upper list) and at D3 (lower list). (C) List of the Ingenuity canonical pathways enriched in the comparison between D3 and D0 for WT (left-hand list) and *Trim32* KO (right-hand list) obtained with a score ≥ 9 of −log(*P*-value). Common pathways are shaded in green. (D) Bubble plot of pathways enrichment showing pathways significantly enriched in the comparison between D3 and D0 for either WT or *Trim32* KO. Color indicates *z*-score, bubble size indicates ratio, and X axis indicates adjusted *P*-values obtained from the Ingenuity Pathway Analysis. (E) Heatmap visualization of DEGs involved in the significantly enriched pathways shown in D. Samples of WT and *Trim32* KO clones at proliferation (D0) and early differentiation (D3) stages are shown. Genes are clustered based on expression similarity. Color scale indicates relative expression.

either nondetected or only modestly upregulated in *Trim32* KO clones at D3 (Fig. 3A). This genotype-specific disparity was further confirmed by gene set enrichment barcode plots, which demonstrated significant enrichment of these muscle-related transcripts in WT cells (FDR_UP = 0.0062), but not in *Trim32* KO cells (FDR_UP = 0.24) (Fig. 3B). These findings support an early transcriptional basis for the impaired myogenesis previously observed in *Trim32* KO cells. Some of the genes detected as de-regulated in the transcriptomic profiles and belonging to the Sarcomere pathway were also analyzed by real-time RT-PCR and this analysis confirmed their significant differential expression only at D3 and not at D0, further supporting the fact that Trim32 contribution becomes more relevant as differentiation progresses (Fig. 3C, left-hand side). In addition to differences in muscle-specific gene expression, we observed that also several pathways related to cell proliferation and cell cycle regulation were more enriched in *Trim32* KO cells compared to WT as suggested by the Ingenuity Pathway Analysis. We therefore also tested the relative expression of some genes implicated in cell cycle to validate the involvement of this pathway. Also in this case, we observed similar level of expression between WT and Trim32 KO cells in growing conditions (D0) but their differential expression at D3 of differentiation, further supporting proliferation and cell cycle control as one of the main pathways affected by lack of Trim32 (Fig. 3C, right side). This suggests that altered cell proliferation may contribute to the distinct differentiation behavior observed in *Trim32* KO versus WT. Given that cell cycle exit is a critical prerequisite for the onset of myogenic differentiation and considering that previous studies on Trim32 role in cell cycle regulation have reported inconsistent findings, we further examined cell cycle dynamics under our experimental conditions to clarify Trim32 contribution to this process.

Trim32 regulates cell cycle exit during the transition from proliferation to differentiation

At the onset of myogenic differentiation, a complex MRFs regulatory network induces cells to reduce their proliferation rate to eventually exit the cell cycle, a prerequisite to start the differentiation program [44,45]. Given the observed dysregulation of pathways related to cell cycle and proliferation in *Trim32* KO clones, we further investigated the role of Trim32 in regulating cell cycle dynamics during this critical transition.

We thus assessed the positivity for phospho-histone H3 (Ser10, pHH3), as a marker of mitosis, under growth conditions (D0) and 2 days after differentiation onset (D2). At D0, similar percentages of pHH3-positive myoblasts were observed in *Trim32* KO and WT C2C12 cells, indicating comparable mitotic rates under proliferating conditions (Fig. 4A, upper panels and graph). Upon differentiation induction, proliferation slowed down in both *Trim32* KO and WT clones, as evidenced by a decrease in the percentage of pHH3-positive myoblasts from D0 to D2. However, at day 2, a significantly higher percentage of pHH3-positive myoblasts was observed in *Trim32* KO clones compared to WT, indicating the presence of a more significant number of *Trim32* KO cells still undergoing mitosis (on average 1.2% of KO cells compared to 0.2% in WT) (Fig. 4A, lower panels and graph). Consistently, MTT assay also showed that *Trim32* KO cells maintained a higher metabolic activity even after differentiation was induced suggesting a potential impairment in cell cycle withdrawal at the onset of myogenesis (Fig. 4B).

At this point, we analyzed cell cycle progression by flow cytometry to discriminate cells in the various phases of the cell cycle. In proliferative conditions (D0), we observed no difference between WT and *Trim32* KO clones when considering the percentage of cells in either phase of the cell cycle. Likewise, upon

culturing for two further days in growth medium (GM D2) we observed a similar increase in percentage of cells in the G1 phase accompanied by a decrease of percentage of cells in the S and G2/M phases with no differences between genotypes, indicating that absence of Trim32 does not affect contact inhibition-induced cell cycle withdrawal. The effect of Trim32 ablation was however evident when analyzing cell cycle

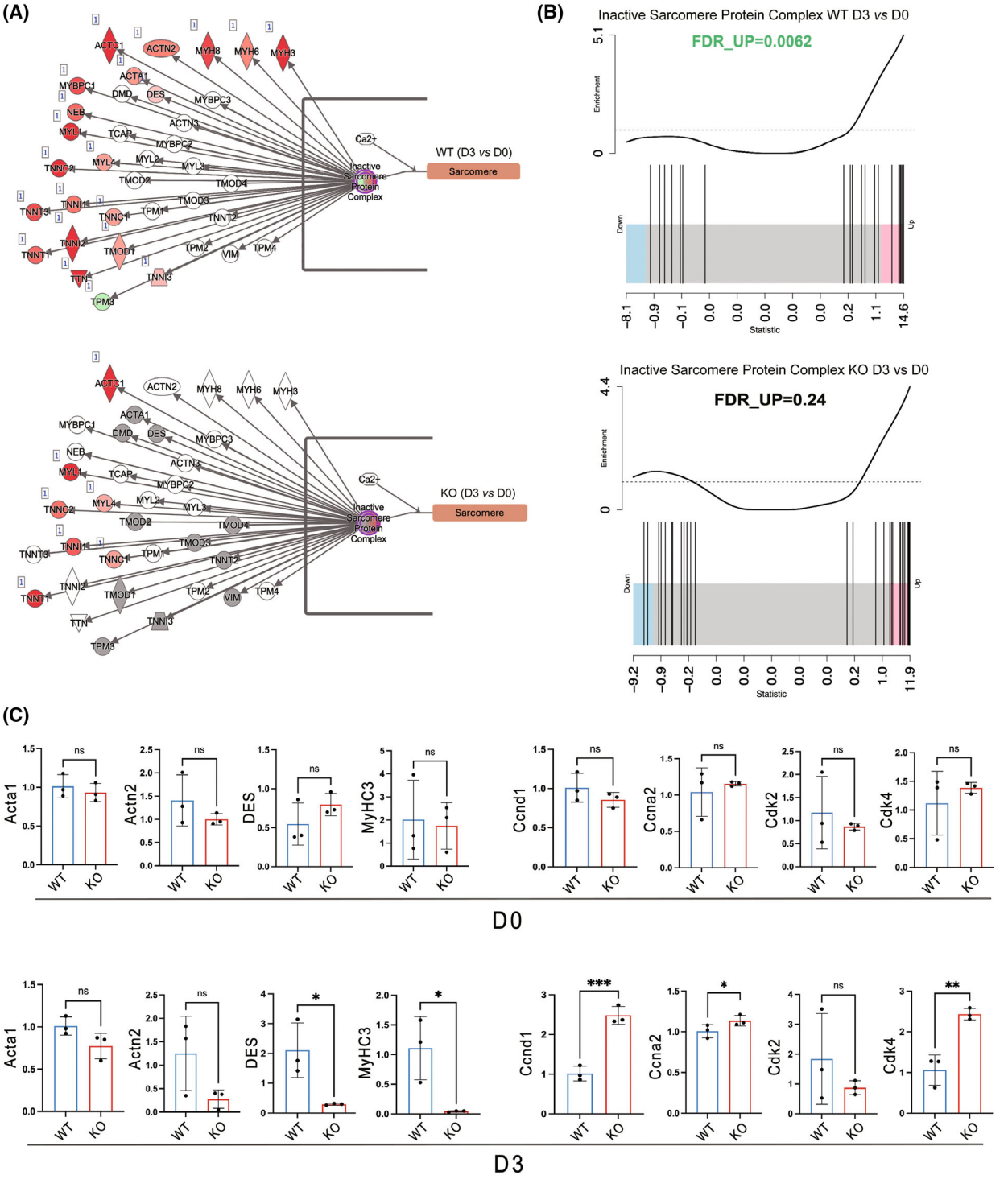

Fig. 3. Transcriptional analyses of cell cycle and sarcomere genes in wild-type (WT) and *Trim32* knock-out (KO) clones. (A) Expression changes of genes belonging to the Inactive Sarcomere Protein Complex pathway from D0 to D3 in WT (upper scheme) and *Trim32* KO (lower scheme). Red symbols indicate upregulation between D3 and D0, green symbols indicate downregulation, gray symbols indicate no statistically significant difference between D3 and D0, and white symbols indicate genes that were not detected. (B) Gene set enrichment barcode plots show the expression change of each gene within the Inactive Sarcomere Protein Complex pathway after 3 days of differentiation in WT (FDR_UP = 0.0062) and *Trim32* KO (FDR_UP = 0.24). (C) Validation of some differentially expressed genes related to the sarcomere process (*Acta1*, *Acta2*, *DES*, and *MyHC3*) and to cell cycle (*Ccnd1*, *Ccna2*, *Cdk2*, and *Cdk4*) in WT and *Trim32* KO clones analyzed by real-time RT-PCR at D0 (upper graphs) and D3 (lower graphs) (mean ± SEM; $n = 3$, unpaired t-test, $*P < 0.05$, $**P < 0.01$, $***P < 0.001$). Relative mRNA expression was calculated using the $2^{-\Delta\Delta Ct}$ method. Ct values were normalized to *Gapdh*, and the mean ΔCt value of the three WT clones was used as the reference.

withdrawal induced by the differentiation stimulus. When compared to growth in proliferating conditions (GM D2), serum depletion in WT clones caused in fact a further increase of cells in G1 phase, and a subsequent decrease of cells in the S and G2/M phases. These changes indicate that WT cells respond to differentiation cues by promptly withdrawing from the cell cycle in order to initiate the differentiation program. In *Trim32* KO clones, however, this differentiation-induced proliferation arrest was less pronounced, and indeed, if compared to WT, the *Trim32* KO clones showed a lower percentage of cells in the G1 phase and a higher percentage of proliferating (S and G2/M phases) cells after two days in differentiation medium (DM D2), indicating a higher proliferation rate (Fig. 4C). To further support this, we used Carboxyfluorescein Diacetate Succinimidyl Ester (CFSE) to monitor cell division. CFSE covalently labels cytoplasmic proteins with a fluorescent dye, and during cell division, the marker is equally distributed between daughter cells, resulting in reduced fluorescence intensity. Thus, cell proliferation can be quantified by measuring the fluorescence dilution using flow cytometry. At 2 days postinduction of differentiation, *Trim32* KO clones exhibited a significantly higher proliferation index compared to WT clones further confirming the above results (Fig. 4D,E).

Overall, these results indicate that Trim32 deficiency interferes with proper and timely cell cycle exit in response to the differentiation stimulus, likely delaying the initiation and/or the extent of differentiation in C2C12 cells.

Trim32 regulates c-Myc mRNA stability during cell cycle withdrawal

c-Myc proto-oncogene plays a crucial role in regulating cell fate and proliferation across various cell types, including C2C12 myoblasts [46,47]. Notably, sustained c-Myc expression in C2C12 myoblasts inhibits myotube formation, and its downregulation is necessary to promote differentiation [47–49]. Indeed, in C2C12 parental cells we observed a progressive reduction in c-Myc levels during the course of differentiation and notably, c-Myc downregulation was induced within hours of serum depletion, indicating that it is one of the first events leading to the differentiation process (Fig. 5A). Similarly, in both WT and *Trim32* KO clones, western blot analysis revealed indeed significant reduction in c-Myc levels after 6 h in differentiation medium. However, c-Myc levels remained relatively higher in *Trim32* KO clones compared to WT clones at this stage (Fig. 5B). Further consolidating the functional meaning of the observed different levels of c-Myc, transcriptional analysis of known c-Myc downstream target genes [50] after 3 days of differentiation confirmed that the observed higher levels of c-Myc correlate with its elevated activity, since three of the genes activated by c-Myc—*Ccnb1*, *Rcl*, and *Tnbs1*—all showed higher levels in *Trim32* KO clones, while three of the genes inhibited by c-Myc—*Adm*, *Eca40*, and *Tert*—exhibited lower transcript levels in *Trim32* KO clones (Fig. 5C). Thus, in the absence of Trim32, c-Myc fails to be properly downregulated at differentiation onset, and these augmented levels correlate with enhanced c-Myc transcriptional activity. This sustained expression of c-Myc observed in *Trim32* KO clones might account for the delayed and aberrant differentiation observed in *Trim32* KO myotubes. Indeed, transient overexpression of c-Myc at the onset of differentiation in C2C12 parental cells results in reduced expression of MyHC level in terminally differentiated myotubes, indicating that even slight and temporary perturbations of c-Myc levels during early phases of differentiation may have consequences also in later stages (data not shown).

Previous studies suggested that Trim32 interacts with and ubiquitinates c-Myc, leading to its proteasome-mediated degradation, and this process is necessary to induce muscular and neuronal differentiation [12,28,34,35]. Based on these reports and since we observed sustained expression of c-Myc in differentiating *Trim32* KO C2C12, we hypothesized that also in our experimental system Trim32 could promote C2C12

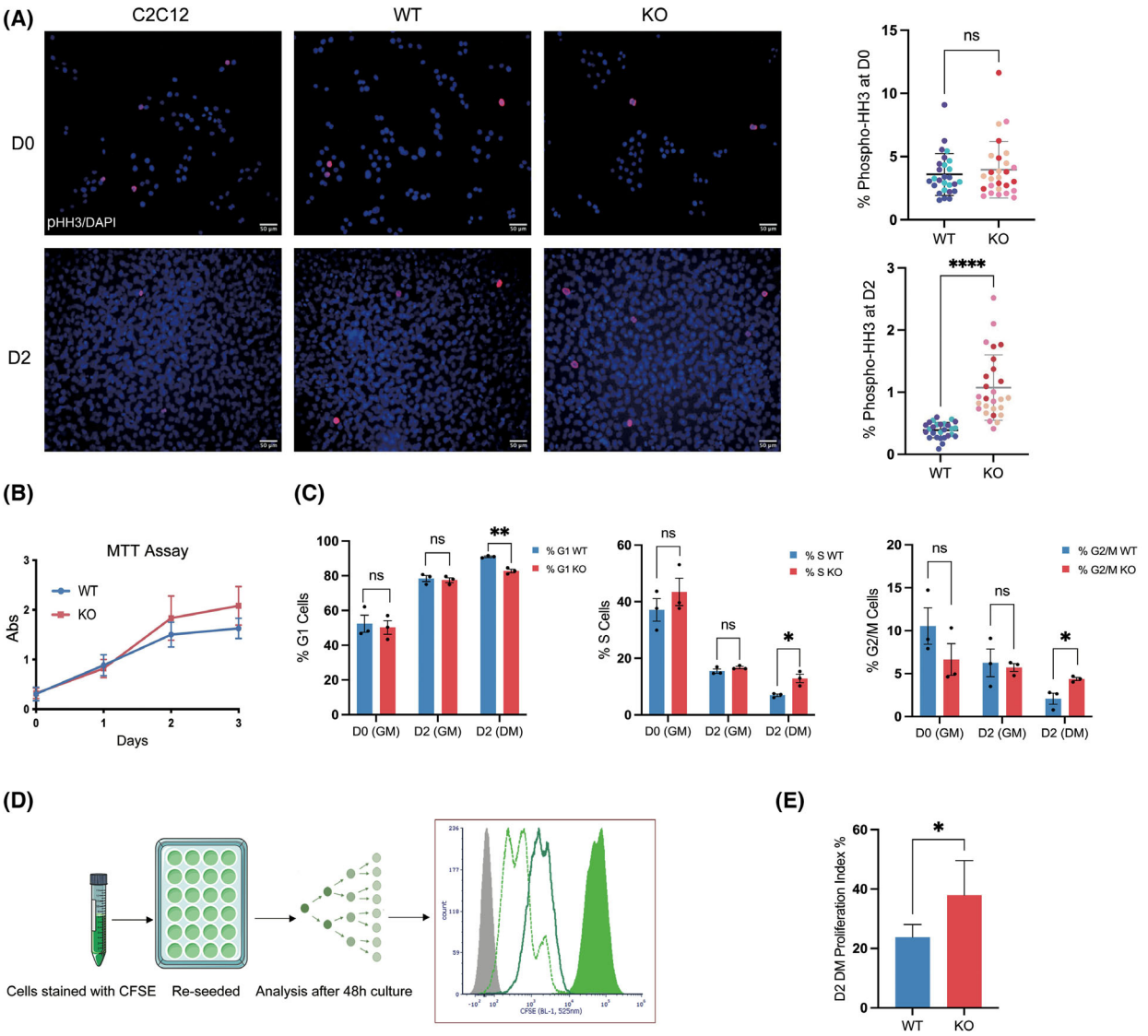

Fig. 4. *Trim32* knock-out (KO) cells exhibit prolonged proliferation after the onset of differentiation. (A) Phospho-histone H3 (pHH3, red) immunostaining. Images of representative wild-type (WT) and *Trim32* KO clones, and C2C12 parental cells in proliferation (D0) and after 2 days of differentiation (D2) (Scale bar = 50 μm; magnification 20×). On the right side, graphs of the corresponding quantification; each dot represents a microscope field (3 fields × 3 coverslips were analyzed for each clone); shades of blue and red represent the different clones (n = 3; mean ± SD; unpaired t-test, ****$P < 0.0001$). (B) Graph representing MTT assay performed to evaluate cell metabolic activity. Cells were cultured in differentiation medium (DM) for the indicated time points and absorbance at 570 nm was measured after MTT addition (mean ± SEM; n = 3). (C) Flow cytometry quantification of the percentage of cells in G1, S, and G2/M phase for WT and *Trim32* KO clones in growth medium (GM) at Day 0 (D0 (GM)) and Day 2 (D2 (GM)), as well as Day 2 after the induction of myogenic differentiation (D2 (DM)) (mean ± SEM; unpaired t-test, *$P < 0.05$, **$P < 0.01$, n = 3). The experiment was repeated 3 times. (D) Measurement of WT and *Trim32* KO clone proliferation by Carboxyfluorescein Diacetate Succinimidyl Ester (CFSE) dilution. Cells were labeled with CFSE and cultured in DM for 48 h. The exponential axis shows decreased fluorescence after 2 days of culturing, displaying the different proliferating rate in WT and *Trim32* KO clones. Gray area: background noise; Green area: Start generation; Dark green line: WT cells; Light green dotted line: *Trim32* KO cells. (E) Graph showing the proliferation index in *Trim32* KO and WT clones using CFSE 2 days after initiating differentiation (D2 DM) (mean ± SEM; n = 2; unpaired t-test, *$P < 0.05$). The experiment was repeated three times.

cell cycle withdrawal by facilitating c-Myc degradation. To test whether Trim32 could promote c-Myc proteasomal degradation, we first treated both WT and *Trim32* KO clones with the proteasome inhibitor MG132 and checked for the accumulation of c-Myc. Of note, c-Myc protein accumulated in both

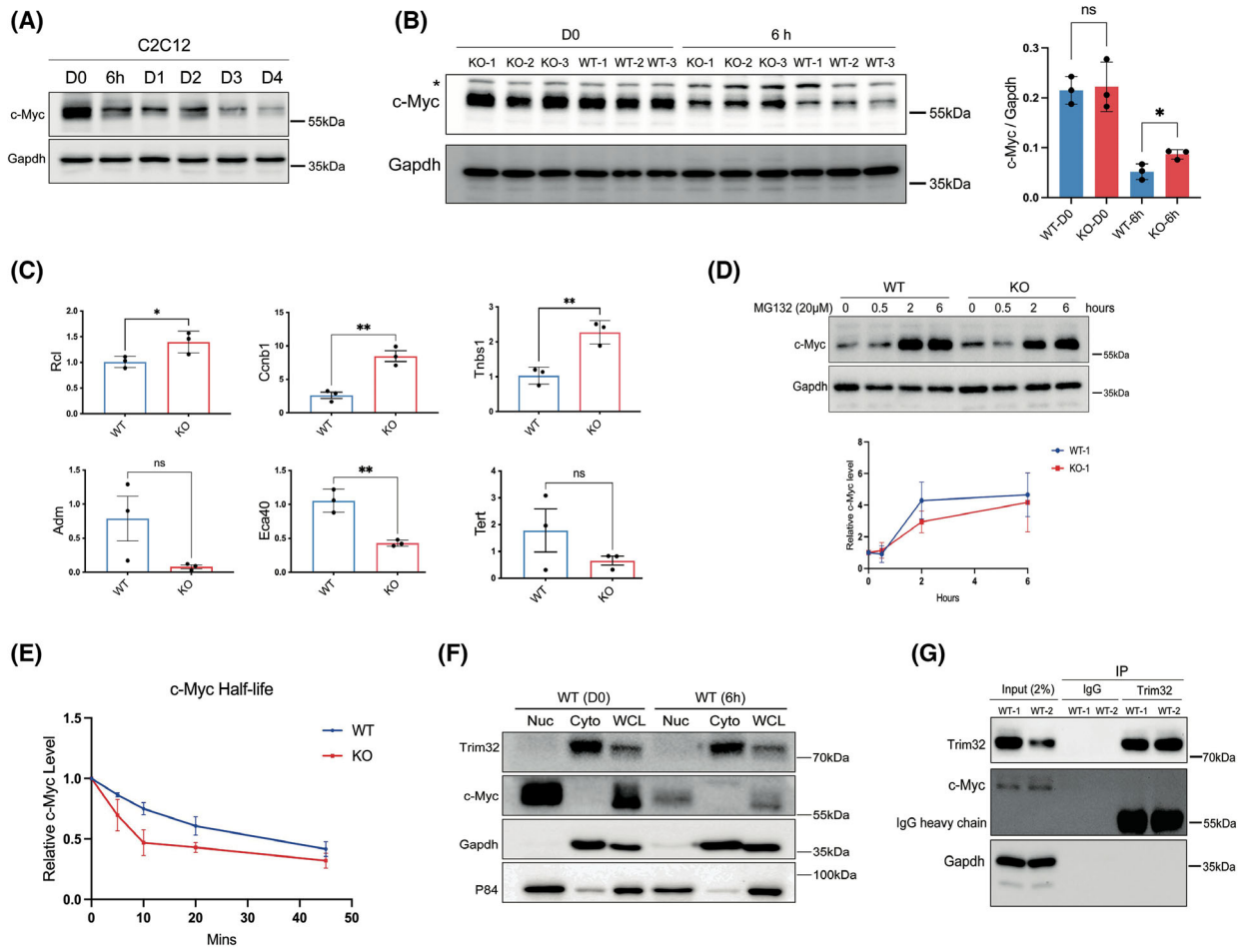

Fig. 5. Trim32 regulates c-Myc level and activity at the onset of C2C12 differentiation. (A) Western blot analysis of c-Myc protein levels in parental C2C12 at D0, and at different time points during differentiation (6 h, D1, 2, 3, and 4). Gapdh was used as loading control. The experiment was repeated twice. (B) Representative western blot analysis of c-Myc in *Trim32* knock-out (KO) and wild-type (WT) clones at D0 (in growth medium (GM)) and 6 h after the induction of myogenic differentiation. Asterisk indicates a nonspecific band. On the right side, graph of the corresponding quantification (mean ± SD; $n = 3$; unpaired t-test, $*P < 0.05$). The experiment was repeated three times. (C) Transcriptional changes of c-Myc downstream target genes in WT and *Trim32* KO clones analyzed by real-time RT-PCR after 3 days of differentiation (mean ± SEM; $n = 3$, unpaired t-test, $*P < 0.05$, $**P < 0.01$). Relative mRNA expression was calculated using the $2^{-\Delta\Delta Ct}$ method. Ct values were normalized to Gapdh, and the mean ΔCt value of the three WT clones was used as the reference. (D) Representative western blot analysis of c-Myc in *Trim32* KO and WT clones cultured in differentiation medium (DM) for 6 h hours before treatment with MG132 for the indicated time points. Below is the graph of the quantification of 3 experimental replicates (mean ± SD). (E) Stability of c-Myc protein detected upon Cycloheximide (CHX) chasing assay in WT and *Trim32* KO clones cultured in DM for 6 h before CHX treatment (mean ± SEM; $n = 3$). The experiment was repeated three times. (F) Nuclear (Nuc) and cytoplasmic (Cyto) fractions from WT clones analyzed by western blot for Trim32 and c-Myc. Gapdh and p84 served as markers for proper cytoplasmic and nuclear fractionation, respectively. WCL: whole cell lysate. The experiment was repeated three times. (G) Immunoprecipitation (IP) with a Trim32 antibody followed by western blot analysis to detect Trim32 and c-Myc in representative WT clones after 6 h of culture in DM. IP with normal rabbit IgG was used as control. The experiment was repeated three times.

genotypes, indicating that its turnover occurs via the proteasome pathway, but independently of Trim32 (Fig. 5D). To further assess if Trim32 is able to affect c-Myc protein stability, we performed a cycloheximide (CHX) pulse-chase assay at the onset of differentiation. In line with the results obtained with proteasomal inhibition, c-Myc half-life resulted not extended in *Trim32* KO clones when compared to WT, suggesting that Trim32 does not facilitate c-Myc degradation in this context (Fig. 5E). Furthermore, subcellular fractionation in WT C2C12 revealed that c-Myc and Trim32 localize to different cellular compartments,

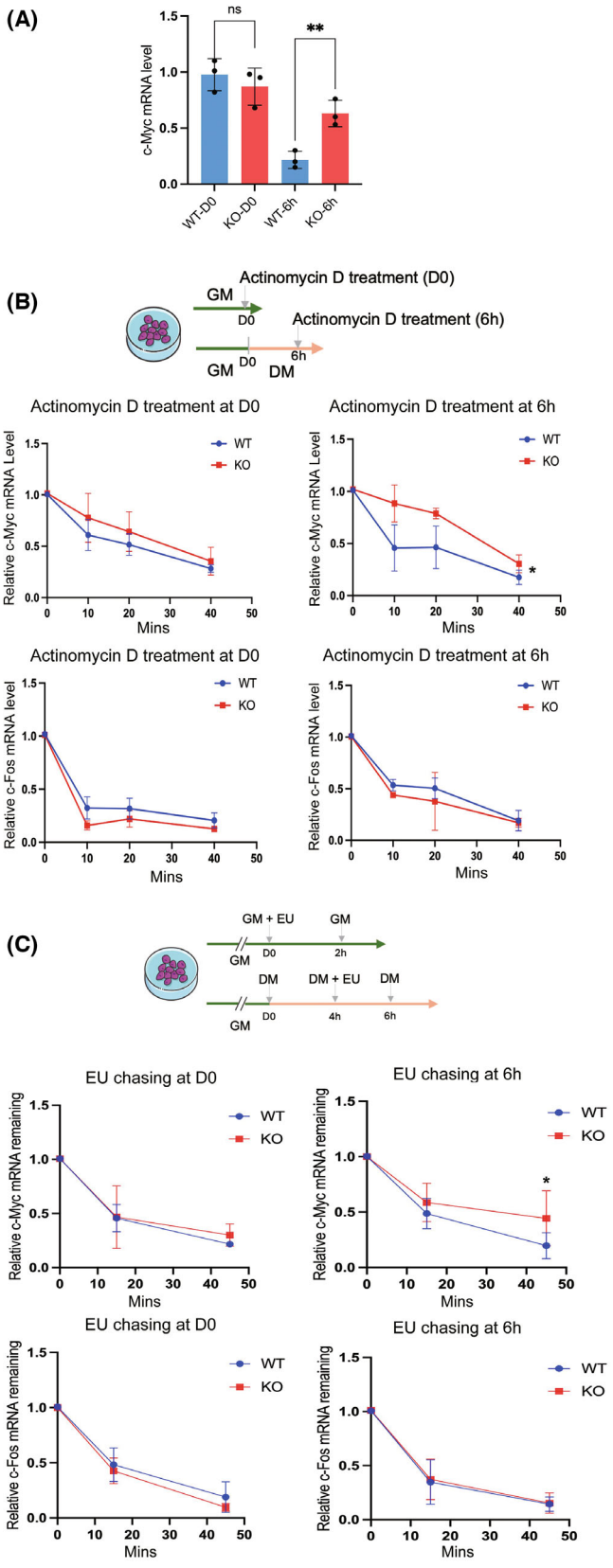

Fig. 6. Trim32 regulates c-Myc level by controlling mRNA stability. (A) Real-time RT-PCR analysis of c-Myc mRNA steady state level in wild-type (WT) and *Trim32* knock-out (KO) clones at D0 and at 6 h of differentiation (6 h) (mean ± SEM; $n = 3$; unpaired *t*-test, $^{**}P < 0.01$). Relative mRNA expression was calculated using the $2^{-\Delta\Delta Ct}$ method. Ct values were normalized to Gapdh, and the mean ΔCt value of the three WT clones was used as the reference. (B) Stability of c-Myc and c-Fos mRNA determined by Actinomycin D chase in WT and *Trim32* KO cells, cultured either in growth medium (GM) (D0) or differentiation medium (DM) for 6 h, for the indicated time points. Relative RNA levels were measured by real-time RT-PCR normalized to Gapdh level (mean ± SEM; $n = 3$; two-way ANOVA, $^{*}P < 0.05$). mRNA levels were normalized to Gapdh expression and expressed relative to 0 h, which was set to 1, using the $2^{-\Delta\Delta Ct}$ method. (C) Stability of nascent c-Myc and c-Fos mRNA determined by 5-ethynyl Uridine (EU) chase in WT and *Trim32* KO cells, cultured either in GM (D0) or DM for 6 h, for the indicated time points. Relative RNA levels were measured by real-time RT-PCR normalized to Gapdh level (mean ± SEM; $n = 3$; unpaired *t*-test, $^{*}P < 0.1$ at 45-min time point). mRNA levels were normalized to Gapdh expression and expressed relative to 0 h, which was set to 1, using the $2^{-\Delta\Delta Ct}$ method.

that is nucleus and cytoplasm, respectively, at both D0 and after 6 h upon the differentiation stimulus (Fig. 5F). Consistently, immunoprecipitation experiments performed after 6 h of differentiation failed to detect any interaction between Trim32 and c-Myc (Fig. 5G). Together, these findings suggest that in the early phases of differentiation, Trim32-mediated c-Myc regulation does not occur post-translationally, and that the increased c-Myc levels detected in *Trim32* KO clones at the onset of differentiation are thus unlikely due to enhanced protein stability resulting from Trim32 ablation.

Growing evidence has demonstrated that members of the TRIM-NHL family, to which Trim32 belongs, can regulate targets' expression by binding to their respective mRNA [10]. We therefore hypothesized that Trim32 might regulate c-Myc abundance by acting at the post-transcriptional level. Real-time RT-PCR analysis shows that, as already observed for the c-Myc protein, also its transcript is promptly downregulated at the onset of differentiation. In *Trim32* KO clones, however, this physiological reduction is less pronounced, suggesting that Trim32 may indeed destabilize c-Myc mRNA in order to reduce its expression (Fig. 6A). Interestingly, no difference between WT and *Trim32* KO clones in c-Myc RNA level is observed in proliferating conditions (D0), indicating that Trim32 regulation is occurring specifically in the early phases of differentiation. To prove this hypothesis, we therefore used Actinomycin D pulse-chase treatment to inhibit transcription and measure c-Myc mRNA half-life in both proliferating conditions and 6 h after switching to DM. Indeed, Trim32 has no effect on the stability of c-Myc mRNA in proliferating conditions, but upon induction of differentiation, the stability of c-Myc mRNA resulted enhanced in *Trim32* KO clones (Fig. 6B). The stability of the c-Fos mRNA, analyzed as control, was not affected by Trim32 in either condition (Fig. 6B). To further support these data, we investigated c-Myc transcript stability also using 5-Ethynyl Uridine (EU) pulse labelling of nascent RNA and chase and capture at different time points, at both D0 and upon 6 h in DM, followed by quantitative analysis with real-time RT-PCR. We indeed confirm that in the absence of Trim32, and only at the onset of differentiation, c-Myc transcript is more stable, again with no effect on c-Fos transcript (Fig. 6C). The enhanced stability of c-Myc transcript at this precise stage of differentiation can explain the elevated levels of c-Myc protein observed in *Trim32* KO clones despite no change of protein stability in these samples and may correlate with delayed cell cycle exit observed in the absence of Trim32.

In summary, these findings suggest that, at differentiation onset, Trim32 regulates c-Myc levels primarily by mRNA destabilization rather than through direct interaction or protein degradation, and that persistent c-Myc protein level in this phase of the differentiation in the absence of Trim32 is due, at least in part, to enhanced c-Myc mRNA stability. We propose that this regulation might be essential for proper cell cycle exit and subsequent myogenic differentiation.

Counteracting c-Myc sustained expression partially rescues Trim32 KO defects

Sustained c-Myc levels observed in *Trim32* KO clones may influence the transition from proliferation to differentiation and result in defective myogenic program activation and aberrant myotube formation. Indeed, myogenic cells overexpressing c-Myc fail to upregulate Myogenin [43,48]. In keeping with these observations, reduced upregulation of Myogenin is indeed observed during differentiation in cells lacking Trim32 expression, as shown above. To further validate the involvement of the Trim32-c-Myc axis in differentiation, we analyzed Myogenin expression in *Trim32* KO upon c-Myc silencing in an attempt to rescue the differentiation defect observed in the *Trim32* KO clones. c-Myc downregulation was achieved by transfecting siRNA into proliferating *Trim32* KO cells, and silencing was validated via real-time RT-PCR and western blot after

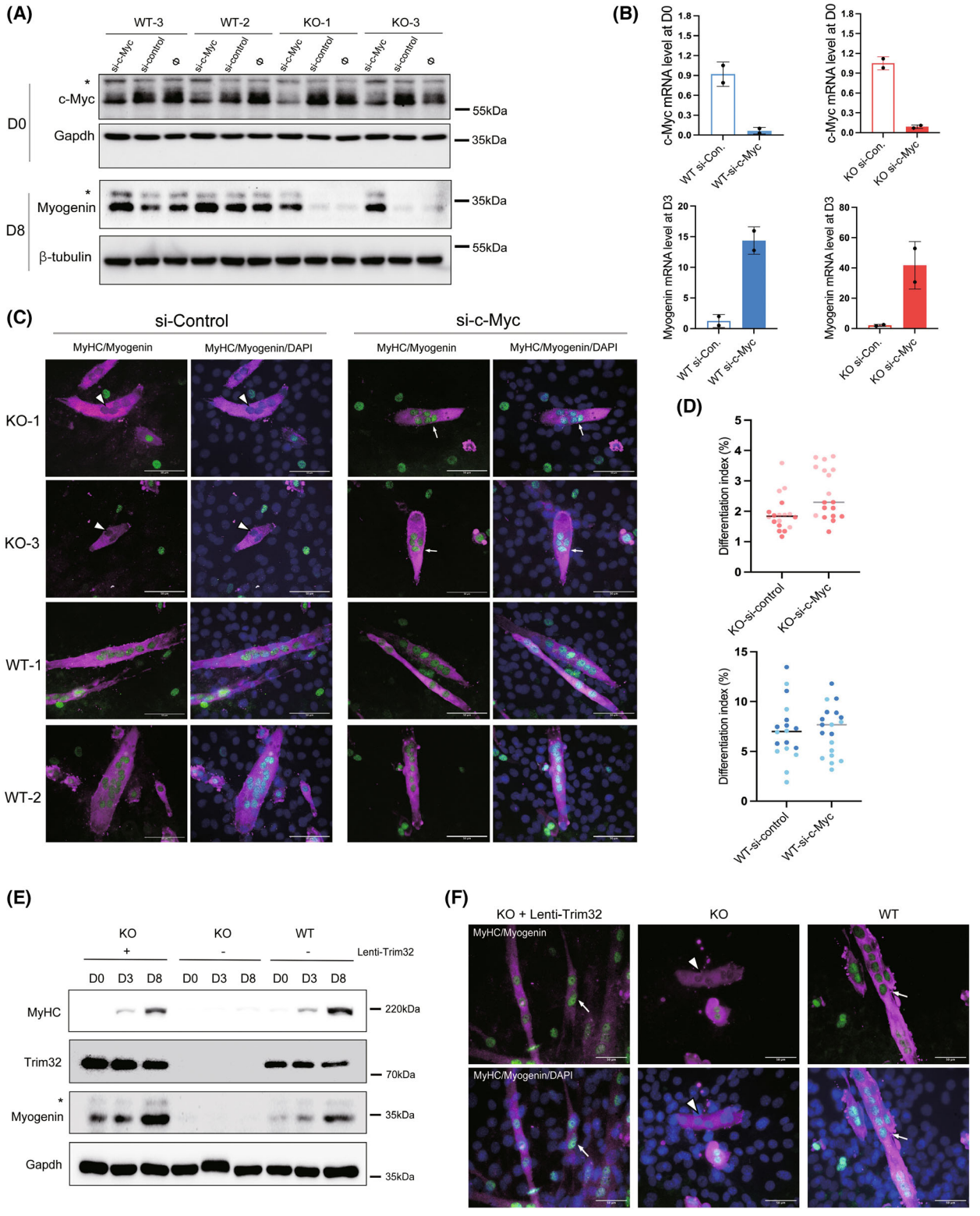

Fig. 7. c-Myc silencing partially rescues *Trim32* knock-out (KO) defects. (A) Representative western blot analysis of wild-type (WT) and *Trim32* KO clones transfected with si-c-Myc, si-Control, and without siRNA. c-Myc levels were detected 24-h post-transfection in growth medium (GM) (D0) (upper panel); myogenin levels were detected at 8 days of differentiation (lower panel). Asterisk indicates a nonspecific band. (n = 2). The experiment was repeated three times. (B) c-Myc (upper graphs) and Myogenin (lower graphs) transcriptional levels were detected in WT and *Trim32* KO cells upon transfection with control siRNA (WT-si-con and KO-si-con) and with c-Myc siRNA (WT-si-c-Myc and KO-si-c-Myc). c-Myc mRNA was detected by real-time RT-PCR after 24 h of culture in GM (D0), and myogenin was detected at 3 days (D3) of differentiation (mean ± SD; n = 2). Relative mRNA expression was calculated using the $2^{-\Delta\Delta Ct}$ method. Ct values were normalized to Gapdh, and the mean ΔCt value of the two si-con was used as the reference. (C) Immunostaining for MyHC (magenta) and Myogenin (green) of WT and KO clones as indicated, upon silencing with control siRNA (si-Control), or c-Myc siRNA (si-c-Myc) at 8 days of differentiation. Arrowheads indicate myotubes displaying nuclei lacking myogenin in *Trim32* KO-si-control, while arrows indicate Myogenin-positive nuclei in *Trim32* KO-si-c-Myc myotubes. Nuclei are counterstained with DAPI (blue) (Scale bar = 50 μm; magnification 63×; n = 2). (D) Graphs reporting the Differentiation index of the experiment represented in panel C. The differentiation index is calculated as the ratio of nuclei within myosin heavy chain 3 (MyHC)-positive myotubes to the total number of nuclei. Each dot represents a 20× microscope field (3 fields × 3 coverslips were analyzed for each clone); shades of red and blue represent the different clones. (E) Representative western blot analysis *Trim32* KO cells transduced with *Trim32*-expressing lentivirus (+) or with a control (−) in parallel to WT cells transduced with the control (−). MyHC, Trim32, and myogenin levels were analyzed at D0, D3, and D8 of differentiation as indicated. Asterisk indicates a nonspecific band. The experiment was repeated three times. (F) Immunostaining for MyHC (magenta) and myogenin (green) of *Trim32* KO cells transduced (KO + Lenti-Trim32) or not (KO) with *Trim32*-expressing lentiviruses in parallel to WT cells after 8 days of differentiation. Arrowheads indicate myotubes displaying nuclei lacking myogenin, while arrows indicate myogenin-positive nuclei. Nuclei are counterstained with DAPI (blue) (Scale bar = 50 μm; magnification 63×; n = 2).

24 h in growth medium (D0) (Fig. 7A, upper panel and 7B, upper graphs). Of note, downregulation of c-Myc in the *Trim32* KO clones was sufficient to greatly elevate Myogenin RNA levels at D3 of differentiation and this transcriptional increase resulted in a full rescue of Myogenin at protein level in *Trim32* KO cells at later stages of differentiation (D8) (Fig. 7A, lower panel and Fig. 7B, lower graphs). These results are consistent with the notion that Myogenin upregulation is prevented by c-Myc sustained expression during myogenesis [48]. Immunostaining further revealed that downregulation of c-Myc in *Trim32* KO clones can not only increase Myogenin levels, but also restore its expression in nuclei of myotubes, as observed in WT cells (Fig. 7C).

However, c-Myc downregulation can only partially improve cell differentiation but it is not sufficient to fully rescue myotube morphology in *Trim32* KO to WT level. Indeed, differentiation index analysis shows that the observed increase is not statistically significant (Fig. 7D). This indicates that Trim32 role during myogenesis is not restricted to the control of c-Myc activity at the onset of differentiation. Indeed, reintroducing Trim32 via lentiviral transduction in KO cells can rescue Myogenin and MyHC expression to levels comparable to those of WT cells (Fig. 7E). Further, upon Trim32 lentiviral transduction, but not in untransduced control, myogenesis is restored with the formation of normal myotubes observable in bright field (data not shown) and with anti-MyHC immunofluorescence staining, in addition to the recovery of nuclear localization of Myogenin in the properly formed myotubes (Fig. 7F).

Together, these findings suggest that precise c-Myc turnover is essential for effective C2C12 differentiation and that the Trim32–c-Myc regulatory axis plays a critical role in the expression of key myogenic factors, particularly Myogenin, within a narrow time window upon the differentiation stimulus.

Discussion

Although mutations in *TRIM32* are widely recognized as the cause of LGMDR8 and an increasing body of evidence from *in vitro* and *in vivo* studies supports a role for Trim32 in muscle regeneration, the precise pathogenic mechanism underlying the disease remains unclear. In this work, we demonstrated that in the C2C12 murine myoblast cell line Trim32 is necessary for full myogenesis by assuring proper cell cycle withdrawal at the very early onset of differentiation. We also showed that Trim32 controls cell cycle exit through the regulation of the stability of the pro-proliferative c-Myc oncogene transcript.

In vivo, muscle regeneration is initiated by skeletal muscle stem cells, the satellite cells, which in adults become activated and exit quiescence going through a phase of proliferation, followed by differentiation and formation of novel myofibers that fuse to existing ones. Studies in *Trim32* KO mouse models and LGMDR8 patients have shown that absence of TRIM32 results in altered satellite cells' biology. In

particular, these appear to be mislocalized within the muscle fibers *in vivo* and to possess a reduced differentiation potential when subjected to *in vitro* differentiation [21,27,28]. However, the reported data are not always concordant and, further, given the complexity of the myogenic process, it is still not clear which steps are directly regulated by TRIM32. To overcome these difficulties, we have generated *Trim32* KO C2C12 myoblast cells as a more homogeneous myoblast model to finely dissect the role of Trim32 in muscular homeostasis.

We have confirmed that the absence of Trim32 in the C2C12 cell line, a myoblast line representing cells at a later commitment stage as compared to muscle satellite cells, results in defective differentiation, characterized by the formation of fewer and smaller myotubes and lower MyHC expression. At the molecular level, the critical role for Trim32 as a regulator of the differentiation process is highlighted by the dramatic impairment in upregulation of key myogenic regulatory factors and genes encoding for sarcomeric proteins observed already in early stages of differentiation at the transcript level in *Trim32* KO cells. These observations are consistent with previous findings in *Trim32* full KO and p.Asp489Asn LGMDR8-associated mutation knock-in mice, which display smaller muscle fibers, small myofibers with centrally located nuclei and a lack of developmental MyHC-positive myotubes, indicating defective muscular regeneration [22,23]. Formation of fewer and abnormally shaped myotubes and reduced expression of differentiation markers such as Myogenin and MyHC was also observed in primary myoblasts from LGMDR8 patients, further confirming the crucial role of TRIM32 for proper myogenesis [21].

Interestingly, our transcriptomic analysis also highlighted differences, between WT and *Trim32* KO clones, in the regulation of cell cycle and proliferation during differentiation. Indeed, we observed that *Trim32* KO clones failed to properly exit the cell cycle upon the serum starvation induction of differentiation and maintained a higher proliferation rate compared to WT clones, even 2-day postdifferentiation onset. Previous reports have already shown that Trim32 is involved in the regulation of cell proliferation; however, most studies have focused on cancer cells with often conflicting results [51–55]. In the context of muscle biology, some studies have investigated *in vitro* differentiation of primary myoblasts isolated from *Trim32* KO animal models or LGMDR8 patients, observing that these cells undergo G0/G1 cell cycle arrest and premature senescence [21,27]. Interestingly, we did not observe such a phenotype in our *Trim32* KO C2C12 cellular model and observed instead an increased proliferation rate that was only evident once cells were prompted to differentiate. It is likely that this discrepancy is due to the fact that those reports referred to senescence of primary satellite cells, while our cellular system represents a myoblast population at a later commitment stage. Of note, this suggests that Trim32 is involved in at least two different steps of myogenesis.

In our model, we found that the inability of *Trim32* knock-out cells to timely exit the cell cycle correlates with inefficient downregulation of c-Myc as early as 6 h after the differentiation stimulus. Indeed, a prerequisite for differentiation is cell cycle exit [56]. This is achieved by rapid downregulation of proproliferative factors, among which is c-Myc [57,58]. Previous studies have shown that a Trim32–c-Myc axis is involved in regulating the balance between proliferation and differentiation in several cellular systems. Studies in the context of neurogenesis showed that Trim32-mediated c-Myc ubiquitination and degradation is a necessary step for neurogenic differentiation [12,35]. Likewise, in the context of myogenesis c-Myc was also shown to be significantly downregulated upon overexpression of Trim32, probably due to its E3 ligase activity [12,28]. Consistent with this earlier view, we found indeed sustained c-Myc expression in *Trim32* KO clones at the onset of differentiation. Surprisingly though, c-Myc protein degradation did not show significant difference in *Trim32* KO and WT clones. Instead, c-Myc transcript level and its stability were increased in *Trim32* KO cells suggesting that Trim32 regulates c-Myc expression by regulating turnover of its transcript rather than protein ubiquitination. The inconsistency with previous data on Trim32-mediated c-Myc ubiquitination and degradation may be due to the specific cell context and/or to the narrow time window we investigated, just after the switch from proliferating to differentiating conditions, where c-Myc abrupt reduction is needed to prompt the myogenesis program. In this context, the proposed potential role for Trim32 in regulating the critical cell cycle exit step during myogenesis is consistent with the observed accumulation of one of its ubiquitin ligase substrates, the NDRG2 protein, in *Trim32* KO muscles. Overexpression of NDRG2 in C2C12 results in delayed cell cycle exit which in turn hinders differentiation, thus providing a further potential molecular mechanism linking Trim32 with regulation of the balance between proliferation and differentiation [59]. It is interesting to note that, differently from other reports, in proliferating conditions, that is, normal serum-containing medium, no effect on proliferation is observed in *Trim32* KO cells.

Regarding the effect on c-Myc mRNA, Trim32 involvement in RNA regulation has been reported, particularly on microRNAs [12], but whether Trim32 directly interacts with c-Myc mRNA or acts through intermediaries such as microRNAs or other proteins, and whether Trim32 E3 ligase activity is required, remains to be determined. Interestingly, some NHL domain-containing TRIM family members have been shown to bind RNA controlling either RNA stability or its translation [9,60]. In this context, we cannot exclude that Trim32 might be also involved in the regulation of c-Myc transcription either directly or indirectly and this will warrant further studies.

Functionally, we demonstrated that c-Myc contributes to the impaired myogenesis observed in *Trim32* KO clones, although this is clearly not the only factor involved in the Trim32-mediated myogenic network; realistically, other molecular mechanisms can participate in this process as also suggested by our transcriptomic results. While downregulating c-Myc at the onset of differentiation restores myogenin expression in nascent myotubes, this intervention is insufficient, at least within our experimental timeframe, to fully normalize the differentiation index or full myotube morphology. Two possible nonexclusive explanations may account for this observation. On one side, c-Myc may influence early stages of myogenesis, such as myoblast proliferation and initial myotube formation, but it may not contribute significantly to later events such as myotube hypertrophy or fusion between existing myotubes and myocytes. This hypothesis is supported by recent work showing that c-Myc is dispensable for muscle fiber hypertrophy but essential for normal MuSC function [61]. Other reports, instead, demonstrated the implication of c-Myc periodic pulses, mimicking resistance-exercise, in muscle growth, a mechanism that cannot though be tested in our experimental model [62,63]. On the other hand, the impaired early onset of myogenesis in *Trim32* KO clones may not result solely from accumulated c-Myc levels. Indeed, Trim32 is known to regulate multiple molecular pathways, and its loss may affect a network of downstream targets beyond c-Myc as also mentioned above and indicated by the transcriptomic approach. Supporting this hypothesis, reintroduction of Trim32 in KO clones is able to fully rescue the myogenic defect, as opposed to the partial rescue observed upon c-Myc silencing. Thus, Trim32 may be involved at various levels of myogenic regulatory pathways, and these different Trim32-dependent mechanisms likely converge to produce the myogenic deficits characteristic of LGMDR8 patients.

In summary, our study demonstrates that the absence of Trim32 disrupts early phases of myogenesis in a cellular system. Further, we identified a novel mechanism through which Trim32 regulates the transition from proliferation to differentiation by modulating c-Myc mRNA stability, revealing an unrecognized pathogenic mechanism that might highlight potential novel therapeutic approaches for future treatment of LGMDR8.

Limitations of the study

This study expands our knowledge of a complex process such as myogenesis and provides further links between TRIM32 and the potential pathogenic mechanism of LGMDR8. However, the primary limitation to the generalization of these results is the use of a single-cell line, albeit well characterized and established for myogenesis research. Future studies should confirm these findings in different experimental systems, such as primary myoblasts or satellite cells, to establish their relevance in the LGMDR8 disease setting. Furthermore, whether c-Myc mRNA regulation by TRIM32 is mediated by direct binding of TRIM32 to the mRNA or indirectly through the activity of other RNA binding proteins or miRNA warrants further investigation. Last, it appears evident that TRIM32 exerts multiple roles during muscular differentiation and likely acts in different phases of the process, as highlighted by the failure of c-Myc silencing to fully restore differentiation as well as by the large number of pathways affected by *Trim32* ablation. Thus, while describing a novel regulatory step in the myogenic process, it appears clear that other effectors must be regulated by TRIM32, and a complete understanding of the role of TRIM32 in myogenesis will be required for the development of targeted therapeutic interventions.

Methods

Cell culture

C2C12 (RRID:CVCL_0188), an immortalized murine myoblast cell line, was a kind gift of Prof. D'Andrea, University of Trieste. Cells were maintained in culture in growth medium (GM): DMEM (Euroclone, ECM0101L), 20% fetal bovine serum (FBS, Gibco, 10 270), 4 mM L-glutamine (Euroclone, ECB3000D), 100 units·mL^{-1} penicillin/100 µg·mL^{-1} streptomycin (Gibco, 15 104). Cells were maintained at 37 °C in 5% CO_2 in a humidified incubator. The C2C12 parental cells used in this study were

maintained within passages 3–8. All clonal cell lines (see below) were utilized within 10 passages following gene editing. In all experiments, WT and *Trim32* KO clones of comparable passage numbers were used to ensure consistency and minimize passage-related variability.

For myogenesis induction, cells were seeded at 50–60% density and cultured in growth medium in either 6 or 10 cm petri dishes. At confluence, GM was replaced with differentiation medium (DM): DMEM (Euroclone, ECM0101L), 2% donor horse serum (biowest, S0900), 4 mM L-glutamine (Euroclone, ECB3000D), 100 units·mL^{-1} penicillin/100 µg·mL^{-1} streptomycin (Gibco, 15 104), counting as Day 0 (D0) of the differentiation process. The DM was changed every day before fixation or cell harvesting according to the different experiments. The differentiation index was calculated as the ratio of nuclei within MyHC-positive myotubes to the total number of nuclei. All experiments were performed with mycoplasma-free cells.

Generation of Trim32 Knock-out clones

Trim32 knock-out C2C12 clones were generated by using the CRISPR/Cas9-based genome editing system (OriGene KN318203D). An all-in-one vector (pCas-Guide) with a *Trim32* target gRNA and Cas9 sequence, and a donor vector (pUC-Donor-vector) carrying GFP-LoxP-Puro-LoxP (Table 2) were transfected into the C2C12 parental cell line using either lipofectamine 3000 (Invitrogen, L3000015) or Mirus TransIT-X2 Dynamic Delivery System (Mirus, MIR6004), as per the manufacturer's recommendations. After 3 weeks of culturing, puromycin (1 µg·mL^{-1}) was applied for selection. The medium was changed every 2–3 days for 10 days and individual cell clones were isolated and expanded. Genomic DNA was extracted from each clone using the PCRBIO Rapid Extract Lysis kit following the manufacturer's instructions (PCRBIOSYSTEMS, PB15.11–24). Genomic DNA was amplified with primers flanking the targeted *Trim32* region (Table 2), and amplicons were Sanger sequenced. Wild-type clones were selected based on the *Trim32* nonmutated sequence.

RNA extraction and RNAseq analysis

Total RNA was extracted with the TRIzol reagent (Thermo Fisher, 15 596–026) following the manufacturer's instructions and was quantified using NanoDrop 2000; for the RNAseq experiments, RNA was also qualitatively evaluated using Agilent Bioanalyzer 2100. RNA was then stored at –80 °C until use.

For the RNAseq experiments, for each of the WT and *Trim32* KO samples at D0 and D3 of the differentiation process, total RNA with an RNA Integrity Number (RIN) higher than 9 was employed. For each sample, libraries were generated starting from 500 ng of total RNA by Illumina Stranded mRNA Prep, according to the manufacturer's protocol. The libraries were quantified using Qubit dsDNA BR Assay Kit on Qubit 2.0 Fluorometer and checked for dimension with DNA 1000 Chip on Bioanalyzer 2100 before pooling. The final sequencing pool was quantified by qPCR before sequencing. Sequencing was performed on NovaSeq 6000 sequencer according to the manufacturer's protocol and generating, for each sample, almost 50 million clusters of 2 × 150 bp paired-end reads. Raw files were subsequently quality checked with FASTQC SOFTWARE and sequences with low-quality score or including adaptor dimers, were discarded from the analysis. The resulting set of selected reads were aligned onto the Mouse genome using STAR version 2.7.3 [65] using GRCm39 Genome Assembly and Gencode.v28 as gene definition. The resulting Mapped reads were used as input for feature Counts functions of Rsubread packages and used as Genes counts for Differential expression analysis using Deseq2 package [66]. Differentially expressed genes (DEGs) were selected for $|\log_2(FC)| -1$ or 1 and corrected *P*-value 0.05 and used as input to perform pathway enrichment analysis by IPA system (Ingenuity® Systems). Gene set enrichment analysis was conducted using the rotation gene set test function within the edgeR package (v 3.38).

RNA pulse and chase

Nascent RNA stability was analyzed by pulse-labeling cells with 5-ethynyl uridine (EU). Cells were seeded in 12-well plates and treated with 0.4 mM EU in either growth medium (GM; D0) or differentiation medium (DM; 6 h) for 2 h, followed by replacement with EU-free medium. Cells were harvested at 0, 15, and 45 min after EU withdrawal, and total RNA was extracted using TRIzol reagent (Thermo Fisher, 15 596–026) according to the manufacturer's instructions. Subsequent procedures were performed using the Click-iT® Nascent RNA Capture Kit (Thermo Fisher, C10365) according to the manufacturer's instructions.

Real time-qPCR

cDNA was reverse transcribed from 1 µg of RNA using SuperScript™ II Reverse Transcriptase (Invitrogen, 18 064 014), according to the manufacturer's instructions, and cDNA stored at −20 °C. RT-PCR was performed using 1/40th of the generated cDNA, SensiFAST™ Probe Kits (Meridian Bioscience, BIO-98020) and 200 nM of forward and reverse primers, in a final volume of 20 µL. Primers were designed to span exons. RT-PCR was performed on a CFX CONNECT SYSTEM real-time PCR machine (Bio-Rad), in technical triplicates. Gene expression changes were calculated using the $2^{-\Delta\Delta Ct}$ method. See Table 2 for primer sequences.

Table 2. Reagents and tools table.

Plasmids

Plasmid name	Source
pUC-Donor-vector KN318203D	OriGene
pCas-Guide	OriGene
pCMV-Flag-c-Myc	[50]
pCMV-Flag	[50]
LV_pPgk1-WPRE	[64]

gRNA sequence

Gene name	gRNA sequence
Trim32	CGGGAAGTGCTAGAAATGT

PCR primers

Gene name	Forward sequence	Reverse sequence
Trim32	GCAGGAATCTGACACTGG	GTCAATGATCTTCAGCACCG

RT-PCR primers

Gene name	Forward sequence	Reverse sequence
c-Myc-1	CGCCCAAATCCTGTACCTCG	TCTTCTTGCTCTTCTTCAGAGTCG
Tert	ATCTACCGCACTTTGGTTGC	AAGCAGCTCAAAGCCAAAAG
Tnbs1	GCATATGTGTGGAAGCAACC	GCGTCCAGTAGGTCTTGGAA
Rcl	AGTGACACAGCCATCCCTGG	AGTGACACAGCCATCCCTGG
Eca40	ACTGGACCCATGAAGACGGA	TGCCTGAGCCGAAGACTTCT
Ccnb1	TGTGTGAACCAGAGGTGGAA	GCGTCTACGTCACTCACTGC
Adm	GCGTCTACGTCACTCACTGC	TAGATCTGGTGGGCCAATTT
GAPDH	GGTGAAGGTCGGTGTGAACGG	GTGGTGCAGGATGCATTGCTG
c-Fos	GTCCCAACCCAGGAGATCAT	GAGATAGCTGCTCTACTTTGCC
Myogenin	GTCCCAACCCAGGAGATCAT	GTCCCAACCCAGGAGATCAT
Ccnd1	GCAGAAGGAGATTGTGCCATCC	AGGAAGCGGTCCAGGTAGTTCA
Ccna2	TTGTAGGCACGGCTGCTATGCT	GGTGCTCCATTCTCAGAACCTG
Cdk2	CAGAGGGGTCCATCAAGCTG	CAGAGGGGTCCATCAAGCTG
Cdk4	CATACCTGGACAAAGCACCTCC	GAATGTTCTCTGGCTTCAGGTCC
Acta1	ACCATCGGCAATGAGCGTTTCC	GCTGTTGTAGGTGGTCTCATGG
Acta2	CACCTGGAGTTTGCCAAGAGAG	CACCTGGAGTTTGCCAAGAGAG
DES	CAACTTCCGAGAAACCAGCC	CATCCCGGGTCTCAATGGTC
MyHC3	CTGGCTAAGTCGGAGGCAAAGA	TCGCATCGTTCCTCAGCATCCA

Antibodies

Antigen	Host species	Company	References
Anti-TRIM32	Rabbit	Proteintech	#10326-1-AP
Anti-TRIM32	Rabbit	GeneTex	#113937
Anti-Myosin Heavy Chain III	Rabbit	Santa Cruz	#sc-20 641
Anti-MyoD1	Rabbit	Proteintech	#18943-1-AP
Anti-Myogenin	Mouse	Santa Cruz	#sc-52 903
Anti-c-Myc	Rabbit	Proteintech	#18028-1-AP
Anti-GAPDH	Mouse	Sigma	#8795
Anti-β-Tublin	Mouse	Sigma	#T4026
Anti-phosphor-Histone3-Ser10	Rabbit	Cell Signaling	#9701
Anti-Flag	Mouse	Sigma	#F-1804
Anti-Mouse HRP	Goat	Millipore	#AP308P

Table 2. (Continued).

Antibodies			
Antigen	Host species	Company	References
Anti-Rabbit HRP	Donkey	Bethyl Laboratories	#A120-208P
FITC-conjugated anti-Mouse	Goat	DAKO	#F0479
Cy3-conjugated anti-Rabbit	Goat	Millipore	#AP132C

Treatments and transfections

Time course experiments to analyze c-Myc protein and c-Myc mRNA stability were performed by treating the cells with 20 μM MG132 (Merck, 474 790), 25 $\mu g \cdot mL^{-1}$ cycloheximide (Thermo Fisher, J66901), and 5 $\mu g \cdot mL^{-1}$ Actinomycin D (Sigma-Aldrich, A1410), respectively. The time of treatment is indicated in the results section.

Plasmid DNA harboring Flag-c-Myc (Table 2), already available in the laboratory, was transfected in C2C12 cells with Lipofectamine 3000 (Invitrogen, L3000015) following the manufacturer's instructions. Cells were harvested 24 h (D0) and 8 days (D8) after induction of differentiation for western blot analyses.

Lentiviral vectors used in this work are based on the pPgk1-EGFP-WPRE vector (control) in which *Trim32* insert was cloned in place of EGFP (LV_pPgk1-HA-Trim32). Lentiviruses were generated and titrated as described in [64]. Cells were seeded in 12-well plates and transduced with Trim32 lentivirus (or control) at a multiplicity of infection (MOI) of 100 in growth medium (GM) supplemented with 10 $\mu g \cdot mL^{-1}$ polybrene. Transduced cells were cultured for 3–4 passages and subsequently switched to differentiation medium (DM) to induce differentiation.

For silencing experiments, siRNA (Dharmacon, FE5L040813000010 and FE5L0018101020) and DharmaFECT reagent (Dharmacon, FE5T200102) were each diluted, combined, and incubated according to the manufacturer's instructions. The transfection mixture was brought to the appropriate volume and added at a final concentration of the siRNA of 25 nM. Cells were harvested 24-h post-transfection in growth medium (D0), as well as at various time points after differentiation induction for RNA and protein analysis.

Immunofluorescence experiments

C2C12 cells were seeded on glass coverslips at a density of 7.5×10^4 $cells \cdot mL^{-1}$. Coverslips were collected at different time points, washed twice in PBS (137 mM NaCl, 2.7 mM KCl, 10 mM Na_2HPO_4, 1.8 mM KH_2PO_4, pH 7.4) and fixed in 4% paraformaldehyde (PFA) in PBS for 15 min at room temperature, or fixed in methanol for 10 min on ice (for myosin heavy chain stain). Cells were then rinsed in PBS and blocked with 5% BSA (VWR Life science, 0332) in PBS-Triton X-100 (0.3%) for 1 h at room temperature. Coverslips were incubated with primary antibodies, diluted in 1% BSA in PBS-Triton X-100 (0.3%), overnight at 4 °C. Staining was obtained after incubation for 1 h at room temperature with a Cy3-conjugated anti-rabbit antibody (1 : 200 dilution, #AP132C; Millipore) or FITC-conjugated anti-mouse antibody (1 : 200 dilution, #F0479; DAKO). Coverslips were mounted with Vectashield mounting medium plus DAPI (Vector Laboratories, H-1200) and cells were imaged with epifluorescence microscopy: 20× magnification images were used to calculate differentiation index and percentage of pHH3 positive cells, while 40× and 63× magnification images were used for more detailed analyses, through ImageJ software (NIH, Bethesda, USA). See Table 2 for antibodies information.

Western blot

Cells were lysed either in RIPA buffer (50 mM Tris/HCl pH 8, 0.3% SDS, 150 mM NaCl, 0.5% Sodium Deoxycholate, 1% NP-40, 1 mM PMSF and 1× Protease Inhibitor Cocktail (Sigma-Aldrich, P8340)) or Myosin extraction buffer (300 mM NaCl, 0.1 M NaH_2PO_4, 0.05 M Na_2HPO_4, 0.01 M $Na_4P_2O_7$, 1 mM $MgCl_2$, 10 mM EDTA, 1 mM DTT, 1 mM PMSF and 1× Protease Inhibitor Cocktail (Sigma-Aldrich, P8340)). Samples were sonicated 5 s × 3 pulses. The insoluble fraction was removed by centrifugation at 20000 × ***g*** for 10 min at 4 °C. Protein quantification was carried on with Bradford assay (Bio-Rad, #500-0006) following the manufacturer's instructions. Proteins were boiled at 95 °C for 5 min in 1× Laemmli buffer supplemented with 5% β-mercaptoethanol and loaded on 7.5%, 10%, or 12% polyacrylamide gels (PAGE), depending on the resolution required, and blotted on PVDF membranes (Millipore, Immobilon-P, IPVH-00010) overnight at 4 °C. Membranes were then blocked in 5% Nonfat dry milk (Cell Signaling Technology, 9999S) in TBS 1× (150 mM NaCl, 10 mM Tris pH 7.4) with 0.1% Tween (TBST), for 1 h at room temperature. Primary antibodies were diluted in 5% Nonfat dry milk in TBST or 5% BSA in TBST and incubated for 2 h at room temperature or overnight at 4 °C. Secondary antibodies were incubated for 1 h at room temperature, diluted in 5% Nonfat dry milk or BSA in TBST. See Table 2 for antibodies information. For detection, membranes were incubated with HRP substrate (ECL

Pierce, Invitrogen, 32 106) for 1 min, and images acquired with ChemiDoc MP Touch Imaging System (Bio-Rad). Relative bands intensities were analyzed by Image Lab software (Bio-Rad).

MTT assay

MTT (Sigma-Aldrich, M2128) was used to determine cells' metabolic activity. Cells were seeded in 96-well plates at a concentration of 6000 cells per well in 200 µL growth medium, in technical triplicate. About 24 h after seeding (D0), 10 µL MTT solution (5 mg·mL^{-1} in PBS; 0.5%) was added to each well and cells were kept incubated at 37 °C for 4 h. After incubation, the medium was removed and 150 µL DMSO (Sigma-Aldrich, 154 938) was added to each well to dissolve the formazan crystals. The absorbance was read by NanoQuant (Infinite M200PRO) at OD = 590 nm. The experiment was carried out with cells at Day 1 (D1), D2, and D3 of differentiation.

Cell cycle and proliferation analysis by flow cytometry

For cell cycle analysis, 7.5 × 10^5 cells were seeded in 10 cm dishes and allowed to adhere overnight in growth medium. The next day, cells were washed twice with PBS, trypsinized and collected in a 15 mL centrifuge tube (D0). Samples were spun down at 125 × ***g*** for 5 min, and the supernatant was discarded, and the cells were resuspended in 500 µL PBS. 1 × 10^6 cells were counted and dropped into 1 mL of EtOH 70%, vortexed, and stored at 4 °C. The same process was carried out with cells grown for 48 h in growth medium or after induction of differentiation.

Before staining, cells were diluted by adding 1 mL PBS and centrifuged at 850 × ***g*** at 4 °C for 5 min. The residual EtOH was removed by rinsing with PBS twice, and cells were then resuspended in 1 mL PBS and stored at 4 °C for 1 h. Afterwards, the PBS was discarded by centrifugation, and cells were resuspended in propidium iodide (PI) staining solution (10 µg·mL^{-1} final concentration) (Sigma-Aldrich, P-4170), incubated overnight at 4 °C, and analyzed using a flow cytometer.

For Carboxyfluorescein Diacetate Succinimidyl Ester (CFSE) tracing cell proliferation, cells were counted and divided into two groups: cells without CFSE for background noise at time 0 and cells stained with CFSE for proliferation analysis; an aliquot of CFSE-stained cells was used for fluorescence intensity analysis at time 0 (starting generation), the remaining fluorescent cells were seeded in growth medium for 48 h before being collected and analyzed for green fluorescence. Staining with the viable probe was performed as follows: CFSE 5 µM was used to label 1 × 10^6 cells. During the first 10 min, CFSE-stained cells were kept in PBS buffer; then the volume was doubled with growth medium to reach the final volume of 1 mL and incubated for another 5 min (all incubations at room temperature). Cells were centrifuged and rinsed with PBS to remove excess CFSE. After the washing step, cells were resuspended for flow cytometric analysis or for culturing. All steps in the presence of CFSE were performed in the dark. PI solution (10 µg·mL^{-1} final concentration) was added to all samples immediately prior to the flow cytometry acquisition and PI-positive cells were excluded from analysis to assess proliferation for undamaged cells only.

All Flow cytometry assays were performed using an Attune NxT instrument (Thermo Fisher Scientific) endowed with acoustic focusing technology, equipped with a blue laser (488 nm, 50 mW) and standard optical bench configuration (4 color channels). After recording at least 20 000 events per run at flow rates of 100 µL·min^{-1} to avoid clumping, data were saved as FCS files and subjected to software analysis using FCS express V7 *De Novo* Software V7 with the functions 'Multicycle' for cell cycle analysis and 'Proliferation fit' for cell division analysis.

Co-immunoprecipitation

Cells were lysed on ice for 30 min in ice-cold modified RIPA buffer (50 mM Tris/HCl pH 8, 150 mM NaCl, 1 mM EDTA, 1% NP-40, 0.25% Sodium Deoxycholate) supplemented with 1 mM PMSF, 1 mM Na_3VO_4, 1 mM NaF, and 1x Protease Inhibitor Cocktail (Sigma-Aldrich, P8340). Lysates were centrifuged at 20 000 × ***g*** for 15 min at 4 °C. Protein concentration was determined by Bradford assay (Bio-Rad, 500-0006). Five percent of each lysate was kept as input sample. Protein A agarose beads (Roche, 11 719 408 001) were equilibrated by washing twice in modified RIPA buffer followed by centrifugation at 850 × ***g*** for 3 min at 4 °C. Equal amounts of equilibrated beads were added to each tube, and samples were incubated on a rotor wheel at 4 °C for 1 h to remove the nonspecifically binding proteins. After centrifugation at 850 × ***g*** for 5 min at 4 °C, 1 µg of antibody (Table 2) was added to the supernatant lysates and samples were incubated on a rotor wheel at 4 °C overnight. The following day, equal amounts of equilibrated beads were added into lysates, and samples were incubated on a rotor wheel at 4 °C for 3 h to pull down the targeted proteins. The beads were then washed four times with modified RIPA buffer followed by centrifugation for 3 min at 850 × ***g*** at 4 °C. The supernatant was set aside as unbound sample. Immunoprecipitates were eluted by boiling at 95 °C for 5 min in 2× Laemmli buffer supplemented with 5% β-mercaptoethanol.

Nuclear/cytoplasmic fractionation

In total, 5 × 10^5 cells were seeded in 6-cm dishes and allowed to reach confluence overnight in growth medium. The next day, the growth medium was replaced with differentiation medium, and cells were cultured for an additional

6 h. Cells were harvested with trypsin–EDTA and then centrifuged at 2300 × ***g*** for 5 min at 4 °C, followed by washing with PBS. The cell pellets were processed using NE-PER Nuclear and Cytoplasmic Extraction Reagents (78 833; Thermo Fisher Scientific) according to the manufacturer's instructions.

Statistics

Unless otherwise indicated, n represents the number of biological replicates (independent clones) in each genotype group. Statistical analyses were conducted using two-tailed unpaired Student's *t*-test and two-way ANOVA, as indicated, using GraphPad Prism 10. Each value represents at least three independent experiments (experimental replicates), except for CFSE tracing cell proliferation, which is the result of two replicates. A *P*-value of < 0.05 was considered statistically significant. *P*-values are denoted as follows: $*P < 0.05$, $**P < 0.01$, $***P < 0.001$, $****P < 0.0001$.

Author contributions

LX: investigation, visualization, writing – original draft, writing – review and editing; EL: conceptualization, investigation, writing – original draft, writing – review and editing; SP: investigation, writing – review and editing; SDM: investigation; EP: investigation, writing – review and editing; DL: conceptualization, formal analysis, writing – review and editing; GM: conceptualization, supervision, funding acquisition, writing – original draft, writing – review and editing.

Acknowledgements

This work has received funding from: European Union's Horizon 2020 research and innovation program under the Marie Skłodowska-Curie grant agreement No 813599 – TRIM-NET; AFM-Telethon, France, grant #23115; and CERIC-ERIC #20242056. L.X. was supported by Fondazione Umberto Veronesi, Italy. We thank Laura Rigoldi for technical support. Meroni's group participates to the COST Action CA20113 – ProteoCure. Schemes used in the figures were adapted from Servier Medical Art (https://smart.servier.com/) licensed under a Creative Commons Attribution 3.0 Generic License. Open access publishing facilitated by Università degli Studi di Trieste, as part of the Wiley - CRUI-CARE agreement.

Conflict of interest

The authors declare no conflict of interest.

Peer review

The peer review history for this article is available at https://www.webofscience.com/api/gateway/wos/peer-review/10.1111/febs.70619.

Data availability statement

Materials of this work are available from the corresponding author upon reasonable request; the raw sequencing data generated in this study have been deposited in the NCBI Sequence Read Archive (SRA) under the accession number PRJNA1280561 (SRA: PRJNA1280561).

References

1 Fridell RA, Harding LS, Bogerd HP & Cullen BR (1995) Identification of a novel human zinc finger protein that specifically interacts with the activation domain of lentiviral tat proteins. *Virology* **209**, 347–357.
2 Reymond A, Meroni G, Fantozzi A, Merla G, Cairo S, Luzi L, Riganelli D, Zanaria E, Messali S, Cainarca S *et al.* (2001) The tripartite motif family identifies cell compartments. *EMBO J* **20**, 2140–2151.
3 Budhidarmo R, Nakatani Y & Day CL (2012) RINGs hold the key to ubiquitin transfer. *Trends Biochem Sci* **37**, 58–65.
4 Joazeiro CA & Weissman AM (2000) RING finger proteins: mediators of ubiquitin ligase activity. *Cell* **102**, 549–552.
5 Napolitano LM, Jaffray EG, Hay RT & Meroni G (2011) Functional interactions between ubiquitin E2 enzymes and TRIM proteins. *Biochem J* **434**, 309–319.
6 Lazzari E, El-Halawany MS, De March M, Valentino F, Cantatore F, Migliore C, Onesti S & Meroni G (2019) Analysis of the Zn-binding domains of TRIM32, the E3 ubiquitin ligase mutated in limb girdle muscular dystrophy 2H. *Cells* **8**, 254.
7 Koliopoulos MG, Esposito D, Christodoulou E, Taylor IA & Rittinger K (2016) Functional role of TRIM E3 ligase oligomerization and regulation of catalytic activity. *EMBO J* **35**, 1204–1218.
8 Tocchini C & Ciosk R (2015) TRIM-NHL proteins in development and disease. *Semin Cell Dev Biol* **47-48**, 52–59.
9 Kumari P, Aeschimann F, Gaidatzis D, Keusch JJ, Ghosh P, Neagu A, Pachulska-Wieczorek K, Bujnicki JM, Gut H, Grosshans H *et al.* (2018) Evolutionary plasticity of the NHL domain underlies distinct solutions to RNA recognition. *Nat Commun* **9**, 1549.
10 Connacher RP & Goldstrohm AC (2021) Molecular and biological functions of TRIM-NHL RNA-binding proteins. *Wiley Interdiscip Rev: RNA* **12**, e1620.

11 Neumuller RA, Betschinger J, Fischer A, Bushati N, Poernbacher I, Mechtler K, Cohen SM & Knoblich JA (2008) Mei-P26 regulates microRNAs and cell growth in the drosophila ovarian stem cell lineage. *Nature* **454**, 241–245.
12 Schwamborn JC, Berezikov E & Knoblich JA (2009) The TRIM-NHL protein TRIM32 activates microRNAs and prevents self-renewal in mouse neural progenitors. *Cell* **136**, 913–925.
13 Frosk P, Weiler T, Nylen E, Sudha T, Greenberg CR, Morgan K, Fujiwara TM & Wrogemann K (2002) Limb-girdle muscular dystrophy type 2H associated with mutation in TRIM32, a putative E3-ubiquitin-ligase gene. *Am J Hum Genet* **70**, 663–672.
14 Weiler T, Greenberg CR, Nylen E, Morgan K, Fujiwara TM, Crumley MJ, Zelinski T, Halliday W, Nickel B, Triggs-Raine B *et al.* (1997) Limb girdle muscular dystrophy in Manitoba Hutterites does not map to any of the known LGMD loci. *Am J Med Genet* **72**, 363–368.
15 Weiler T, Greenberg CR, Zelinski T, Nylen E, Coghlan G, Crumley MJ, Fujiwara TM, Morgan K & Wrogemann K (1998) A gene for autosomal recessive limb-girdle muscular dystrophy in Manitoba Hutterites maps to chromosome region 9q31-q33: evidence for another limb-girdle muscular dystrophy locus. *Am J Hum Genet* **63**, 140–147.
16 Caputo M & Schoser B (2024) The TRIM32 geno-phenotype spectrum: a literature review and 25-year clinical follow-up of two brothers living with sarcotubular myopathy. *Acta Myol* **43**, 139–144.
17 Kumarasinghe L, Xiong L, Garcia-Gimeno MA, Lazzari E, Sanz P & Meroni G (2021) TRIM32 and Malin in neurological and neuromuscular rare diseases. *Cells* **10**, 820.
18 Guan Y, Liang X, Li W, Lin W, Liang G, Xie H, Hou Y, Hu Y & Shang X (2023) TRIM32 biallelic defects cause limb-girdle muscular dystrophy R8: identification of two novel mutations and investigation of genotype-phenotype correlation. *Skelet Muscle* **13**, 10.
19 Neri M, Selvatici R, Scotton C, Trabanelli C, Armaroli A, De Grandis D, Levy N, Gualandi F & Ferlini A (2013) A patient with limb girdle muscular dystrophy carries a TRIM32 deletion, detected by a novel CGH array, in compound heterozygosis with a nonsense mutation. *Neuromuscul Disord* **23**, 478–482.
20 Liang X, Si J, Xie H, Guan Y, Lin W, Lin Z, Zheng G, Wei X, Xiong X, Zhuang Z *et al.* (2025) Investigating genotype-phenotype correlation of limb-girdle muscular dystrophy R8: association of clinical severity, protein biological function and protein oligomerization. *Acta Neuropathol Commun* **13**, 47.
21 Servian-Morilla E, Cabrera-Serrano M, Rivas-Infante E, Carvajal A, Lamont PJ, Pelayo-Negro AL, Ravenscroft G, Junckerstorff R, Dyke JM, Fletcher S *et al.* (2019) Altered myogenesis and premature senescence underlie human TRIM32-related myopathy. *Acta Neuropathol Commun* **7**, 30.
22 Kudryashova E, Struyk A, Mokhonova E, Cannon SC & Spencer MJ (2011) The common missense mutation D489N in TRIM32 causing limb girdle muscular dystrophy 2H leads to loss of the mutated protein in knock-in mice resulting in a Trim32-null phenotype. *Hum Mol Genet* **20**, 3925–3932.
23 Kudryashova E, Wu J, Havton LA & Spencer MJ (2009) Deficiency of the E3 ubiquitin ligase TRIM32 in mice leads to a myopathy with a neurogenic component. *Hum Mol Genet* **18**, 1353–1367.
24 Kudryashova E, Kudryashov D, Kramerova I & Spencer MJ (2005) Trim32 is a ubiquitin ligase mutated in limb girdle muscular dystrophy type 2H that binds to skeletal muscle myosin and ubiquitinates actin. *J Mol Biol* **354**, 413–424.
25 Cohen S, Zhai B, Gygi SP & Goldberg AL (2012) Ubiquitylation by Trim32 causes coupled loss of desmin, Z-bands, and thin filaments in muscle atrophy. *J Cell Biol* **198**, 575–589.
26 Locke M, Tinsley CL, Benson MA & Blake DJ (2009) TRIM32 is an E3 ubiquitin ligase for dysbindin. *Hum Mol Genet* **18**, 2344–2358.
27 Kudryashova E, Kramerova I & Spencer MJ (2012) Satellite cell senescence underlies myopathy in a mouse model of limb-girdle muscular dystrophy 2H. *J Clin Invest* **122**, 1764–1776.
28 Nicklas S, Otto A, Wu X, Miller P, Stelzer S, Wen Y, Kuang S, Wrogemann K, Patel K, Ding H *et al.* (2012) TRIM32 regulates skeletal muscle stem cell differentiation and is necessary for normal adult muscle regeneration. *PLoS One* **7**, e30445.
29 Feng LT, Chen ZN & Bian H (2024) Skeletal muscle: molecular structure, myogenesis, biological functions, and diseases. *MedComm* **5**, e649.
30 Kablar B, Asakura A, Krastel K, Ying C, May LL, Goldhamer DJ & Rudnicki MA (1998) MyoD and Myf-5 define the specification of musculature of distinct embryonic origin. *Biochem Cell Biol* **76**, 1079–1091.
31 Serrano AL, Mann CJ, Vidal B, Ardite E, Perdiguero E & Munoz-Canoves P (2011) Cellular and molecular mechanisms regulating fibrosis in skeletal muscle repair and disease. *Curr Top Dev Biol* **96**, 167–201.
32 Smith CK 2nd, Janney MJ & Allen RE (1994) Temporal expression of myogenic regulatory genes during activation, proliferation, and differentiation of rat skeletal muscle satellite cells. *J Cell Physiol* **159**, 379–385.
33 Hillje AL, Pavlou MA, Beckmann E, Worlitzer MM, Bahnassawy L, Lewejohann L, Palm T & Schwamborn JC (2013) TRIM32-dependent transcription in adult neural progenitor cells regulates neuronal differentiation. *Cell Death Dis* **4**, e976.

34 Hillje AL, Worlitzer MM, Palm T & Schwamborn JC (2011) Neural stem cells maintain their stemness through protein kinase C zeta mediated inhibition of TRIM32. *Stem Cells* **29**, 1437–1447.

35 Nicklas S, Hillje AL, Okawa S, Rudolph IM, Collmann FM, van Wuellen T, Del Sol A & Schwamborn JC (2019) A complex of the ubiquitin ligase TRIM32 and the deubiquitinase USP7 balances the level of c-Myc ubiquitination and thereby determines neural stem cell fate specification. *Cell Death Differ* **26**, 728–740.

36 Jeong SY, Choi JH, Kim J, Woo JS & Lee EH (2023) Tripartite motif-containing protein 32 (TRIM32): what does it do for skeletal muscle? *Cells* **12**, 2104.

37 Shieh PB, Kudryashova E & Spencer MJ (2011) Limb-girdle muscular dystrophy 2H and the role of TRIM32. *Handb Clin Neurol* **101**, 125–133.

38 Delgado I, Huang X, Jones S, Zhang L, Hatcher R, Gao B & Zhang P (2003) Dynamic gene expression during the onset of myoblast differentiation *in vitro*. *Genomics* **82**, 109–121.

39 Yaffe D & Saxel O (1977) Serial passaging and differentiation of myogenic cells isolated from dystrophic mouse muscle. *Nature* **270**, 725–727.

40 Lawson MA & Purslow PP (2000) Differentiation of myoblasts in serum-free media: effects of modified media are cell line-specific. *Cells Tissues Organs* **167**, 130–137.

41 Schiaffino S (2018) Muscle fiber type diversity revealed by anti-myosin heavy chain antibodies. *FEBS J* **285**, 3688–3694.

42 Schiaffino S, Rossi AC, Smerdu V, Leinwand LA & Reggiani C (2015) Developmental myosins: expression patterns and functional significance. *Skelet Muscle* **5**, 22.

43 Wright WE, Sassoon DA & Lin VK (1989) Myogenin, a factor regulating myogenesis, has a domain homologous to MyoD. *Cell* **56**, 607–617.

44 Shen X, Collier JM, Hlaing M, Zhang L, Delshad EH, Bristow J & Bernstein HS (2003) Genome-wide examination of myoblast cell cycle withdrawal during differentiation. *Dev Dyn* **226**, 128–138.

45 Dumont NA, Bentzinger CF, Sincennes MC & Rudnicki MA (2015) Satellite cells and skeletal muscle regeneration. *Compr Physiol* **5**, 1027–1059.

46 Luo W, Chen J, Li L, Ren X, Cheng T, Lu S, Lawal RA, Nie Q, Zhang X & Hanotte O (2019) c-Myc inhibits myoblast differentiation and promotes myoblast proliferation and muscle fibre hypertrophy by regulating the expression of its target genes, miRNAs and lincRNAs. *Cell Death Differ* **26**, 426–442.

47 Seyer P, Grandemange S, Busson M, Carazo A, Gamaleri F, Pessemesse L, Casas F, Cabello G & Wrutniak-Cabello C (2006) Mitochondrial activity regulates myoblast differentiation by control of c-Myc expression. *J Cell Physiol* **207**, 75–86.

48 Miner JH & Wold BJ (1991) c-myc inhibition of MyoD and myogenin-initiated myogenic differentiation. *Mol Cell Biol* **11**, 2842–2851.

49 Denis N, Blanc S, Leibovitch MP, Nicolaiew N, Dautry F, Raymondjean M, Kruh J & Kitzis A (1987) c-myc oncogene expression inhibits the initiation of myogenic differentiation. *Exp Cell Res* **172**, 212–217.

50 Cairo S, De Falco F, Pizzo M, Salomoni P, Pandolfi PP & Meroni G (2005) PML interacts with Myc, and Myc target gene expression is altered in PML-null fibroblasts. *Oncogene* **24**, 2195–2203.

51 Wang C, Xu J, Fu H, Zhang Y, Zhang X, Yang D, Zhu Z, Wei Z, Hu Z, Yan R *et al.* (2018) TRIM32 promotes cell proliferation and invasion by activating beta-catenin signalling in gastric cancer. *J Cell Mol Med* **22**, 5020–5028.

52 Hu Z, Song Q, Ma H, Guo Y, Zhang T, Xie H & Luo X (2021) TRIM32 inhibits the proliferation and migration of pulmonary artery smooth muscle cells through the inactivation of PI3K/Akt pathway in pulmonary arterial hypertension. *J Bioenerg Biomembr* **53**, 309–320.

53 Zhao TT, Jin F, Li JG, Xu YY, Dong HT, Liu Q, Xing P, Zhu GL, Xu H, Yin SC *et al.* (2018) TRIM32 promotes proliferation and confers chemoresistance to breast cancer cells through activation of the NF-kappaB pathway. *J Cancer* **9**, 1349–1356.

54 Cui X, Lin Z, Chen Y, Mao X, Ni W, Liu J, Zhou H, Shan X, Chen L, Lv J *et al.* (2016) Upregulated TRIM32 correlates with enhanced cell proliferation and poor prognosis in hepatocellular carcinoma. *Mol Cell Biochem* **421**, 127–137.

55 Lazzari E & Meroni G (2016) TRIM32 ubiquitin E3 ligase, one enzyme for several pathologies: from muscular dystrophy to tumours. *Int J Biochem Cell Biol* **79**, 469–477.

56 Buttitta LA & Edgar BA (2007) Mechanisms controlling cell cycle exit upon terminal differentiation. *Curr Opin Cell Biol* **19**, 697–704.

57 Bretones G, Delgado MD & Leon J (2015) Myc and cell cycle control. *Biochim Biophys Acta* **1849**, 506–516.

58 Kolly C, Suter MM & Muller EJ (2005) Proliferation, cell cycle exit, and onset of terminal differentiation in cultured keratinocytes: pre-programmed pathways in control of C-Myc and Notch1 prevail over extracellular calcium signals. *J Invest Dermatol* **124**, 1014–1025.

59 Mokhonova EI, Avliyakulov NK, Kramerova I, Kudryashova E, Haykinson MJ & Spencer MJ (2015) The E3 ubiquitin ligase TRIM32 regulates myoblast proliferation by controlling turnover of NDRG2. *Hum Mol Genet* **24**, 2873–2883.

60 Aeschimann F, Kumari P, Bartake H, Gaidatzis D, Xu L, Ciosk R & Grosshans H (2017) LIN41 post-transcriptionally silences mRNAs by two distinct and position-dependent mechanisms. *Mol Cell* **65**, 476–489.

61 Ham DJ, Semeraro M, Berger BM, McGowan TJ, Lin S, Maino E, Oliveri F & Ruegg MA (2025) Muscle fiber Myc is dispensable for muscle growth and its forced expression severely perturbs homeostasis. *Nat Commun* **16**, 3190.
62 Edman S, Jones Iii RG, Jannig PR, Fernandez-Gonzalo R, Norrbom J, Thomas NT, Khadgi S, Koopmans PJ, Morena F, Chambers TL *et al*. (2024) The 24-hour molecular landscape after exercise in humans reveals MYC is sufficient for muscle growth. *EMBO Rep* **25**, 5810–5837.
63 Jones RG 3rd, Edman S, Serrano N, Wen Y, McCarthy JJ, Fry CS, von Walden F & Murach KA (2025) Making sense of MYC in skeletal muscle: location, duration, and magnitude. *Am J Physiol Cell Physiol* **329**, C624–C629.
64 Brancaccio M, Pivetta C, Granzotto M, Filippis C & Mallamaci A (2010) Emx2 and Foxg1 inhibit gliogenesis and promote neuronogenesis. *Stem Cells* **28**, 1206–1218.
65 Dobin A & Gingeras TR (2015) Mapping RNA-seq reads with STAR. *Curr Protoc Bioinformatics* **51**, 1–19.
66 Love MI, Huber W & Anders S (2014) Moderated estimation of fold change and dispersion for RNA-seq data with DESeq2. *Genome Biol* **15**, 550.